Influence of the cross-linking of the cellulosic fibrillar network on the effective hygro-mechanical behavior of the wood cell wall

Nhat-Tung Phan, François Auslender, Joseph Gril, Rostand Moutou Pitti

Acta Mech https://doi.org/10.1007/s00707-022-03355-8 + Erratum Oct 2022

Nhat-Tung PHAN[1] · **François AUSLENDER** · **Joseph GRIL** · **Rostand MOUTOU PITTI**

Influence of the cross-linking of the cellulosic fibrillar network on the effective hygro-mechanical behaviour of the wood cell wall

Abstract

This study aims to analyze the influence of the fibrils oscillations and connections on the effective hygro-elastic behavior of the wood cell wall. For that, two different models of microstructure describing the cell wall are introduced: the model 1S, for which the fibrils are allowed to oscillate in one direction like a sine curve, and the model 2S, for which the fibrils oscillate in two directions as a helix. The effective hygro-elastic behavior of the cell wall associated with each of the two models is computed by numerical periodic homogenization. Then, we analyze the effects of the fibers oscillations on the effective behavior by making vary some parameters such as the shape ratio of the unit cell, the fibrils volume fraction, or the elastic contrast between the matrix and the fibrils. It is shown that the fibrils oscillations have a significant effect on some effective moduli of the cell wall, such as the effective shear moduli $\widetilde{G}_{12}$ (for both model 1S and 2S) and $\widetilde{G}_{13}$, $\widetilde{G}_{23}$ (for model 2S only).

Keywords: effective hygro-mechanical behavior; wood cell-wall; numerical homogenization; finite elements; cross-liking of fibrillar network

1 Introduction

Owing to the structural sophistication and natural variability of wood, the modeling of its structure-properties relationships has always been a challenge for mechanical engineers. Wood anisotropy results from the contribution of various scales of heterogeneity: concentric growth rings with alternation of earlywood and latewood at the macroscopic level, mesoscopic honeycomb-like arrangement of tubular cells, microscopic layering of the cell wall, macromolecular alignment of cellulosic microfibrils [1-3], see Fig. 1. Despite this complexity, a certain amount of organization and regularity exists as a result of the wood formation process and has been the basis of several micro-macro approaches to predict the elastic behaviour, based on a combination of mixture rules and homogenization techniques [2-8].

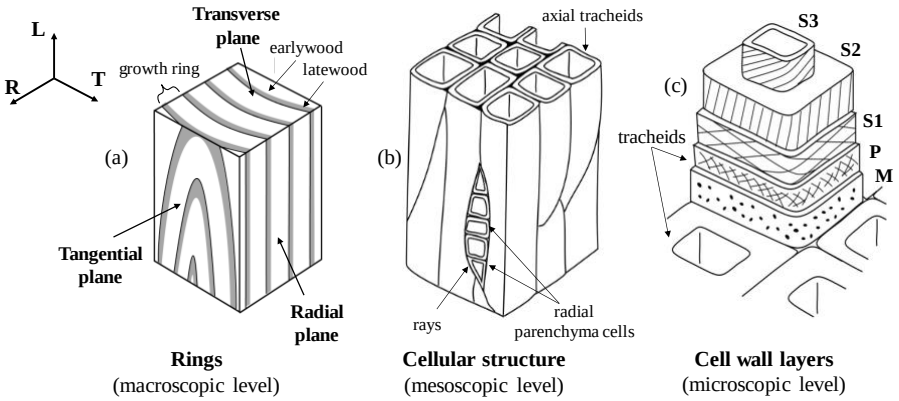

Fig. 1 The schematic structure of a softwood: **a** growth rings layering and principal axes; **b** honeycomb-like cellular tissue; **c** multi-layered cell wall defined by the varying orientation of cellulosic microfibrils

Nhat-Tung Phan · François Auslender (✉) · Joseph Gril · Rostand Moutou Pitti
Université Clermont Auvergne, Clermont Auvergne INP, Institut Pascal, F-63000 Clermont Ferrand, France
E-mail : francois.auslender@uca.fr

Joseph Gril
University Clermont Auvergne, Inrae, Piaf, F-63000 Clermont Ferrand, France

Rostand Moutou Pitti
Cenarest, IRT, BP 14070, Libreville, Gabon

The cell wall is organized in a superposition of layers: the primary layer (P) for which the cellulose fibrils are randomly distributed in its plane, three secondary layers S1, S2 and S3, where the cellulose fibrils have an helicoidal organization with a different microfibril angle (MFA) for each, and a layer called middle lamella ML which joins the cells together. This study will focus on the cell-wall material of the S2 layer, although the approach remains applicable to S1 and S3. According to the representation of Salmén (2004), the cell-wall material is a reinforced fiber composite for which the matrix is a mixture of lignin and xylan hemicelluloses, and the fibers correspond to the macrofibrils; the latter consisting of an assemblage of microfibrils, made themselves of crystalline cellulose, separated by glucomannan hemicelluloses (Fig. 2) [9].

In the literature [2, 3, 6], the macrofibrils have classically been assumed to be straight and parallel to each other (Fig. 2a). However, some experimental characterizations [10, 11] suggest that this is not the case and that the macrofibrils are curved and connected to each other [12]. These suggestions are similar to the models of an oscillating cellulose network originally proposed by Boyd [13], and later used by Gril [14]. Furthermore, this oscillating structure may be the reason for the puzzling orientation interpreted from tomography [15]. As to the nature of the links between macrofibrils, it can be speculated that macrofibrils oscillate by slight deviations from their main direction, and occasionnaly get into contact through hydrogen bonding with neighbouring macrofibrils (Fig. 2b). As an alternative explanation, some of the microfibrils composing a macrofibril could occasionaly shift to the neighbouring one, resulting in stronger connexions (Fig. 2c). In any case, it seems reasonable to assume the existence of a network of macrofibrils laterally connected, separated by lignified matrix incrustations with more or less lenticular shapes. For the sake of simplification, the macrofibrils will be simply be called fibrils in what follows.

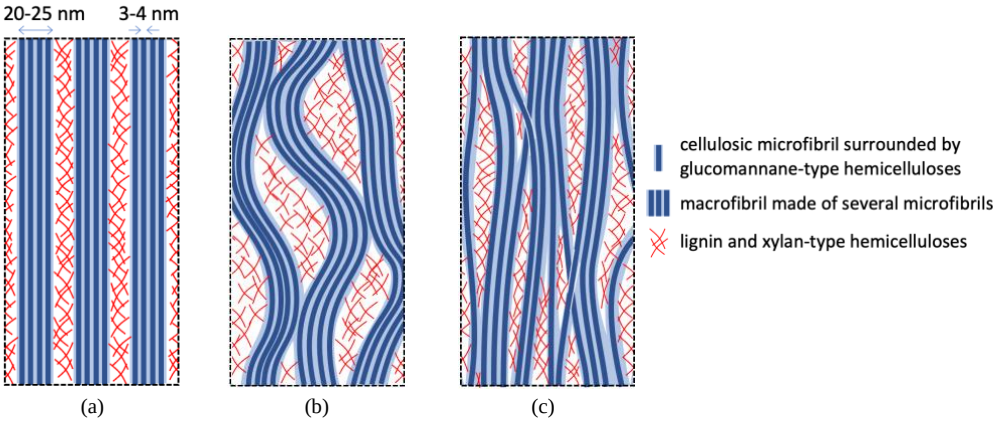

Fig. 2 Interpretation of the interconnexion between macrofibrils: **a** classical representation with straight and parallel microfibrils grouped into macrofibrils separated by lignin matrix; **b** Oscillations and lateral contacts between macrofibrils through hydrogen bonding; **c** connexions resulting from the random transfer of oscillating microfibrils between neighbouring macrofibrils.

The amorphous components of the cell wall (lignin, hemicelluloses and non-crystalline cellulose) are characterized by hygro-thermo-activated viscoelascity, with the softening effect of moisture content [7] triggered by temperature. The glassy transition of lignin falls well below 100°C above the fiber saturation point [16], which is the basis of wood forming techniques [17]. However, even if very high levels of deformation can be obtained with wet and hot wood, the material retains some elasticity: irrecoverable flow is not observed as a result of forming operations, on the contrary almost full recovery occurs through re-softening after unloading [18]. These observations further support the existence of a continuous microfibrillar network in the cell wall, preventing the relative sliding of fibrils separated by a plasticized matrix.

The goal of this study is to explore the consequences of a more realistic description of the morphology of the secondary layers, taking into account both the fibrils oscillations and connections, on the effective hygroelastic behavior of the cell wall. For that, the complex molecular structure of the material constituting each layer of the secondary cell wall will be assumed equivalent to the periodic repetition of an elementary unit containing a simplified distribution of the components considered as continuous media. The effective behavior is then determined by classical numerical homogenization techniques for periodic media, e.g. see Bornert et al [19]. In

order to focus on the morphological effect, the effective behavior of the fibrils will be taken as an input of the model; however, owing to the presence of some glucomanans the possibility of their water-induced expansion will be considered. The viscoelasticity of the matrix will not be modelled and only indirectly taken into account by simulating a considerably reduced modulus. Moreover, although the anisotropy of the matrix is supported by a number of arguments [9], in the proposed models it will be taken as isotropic.

2 Representation of the cell wall microstructure of wood

In this section different models of periodic cell are proposed to stand for the morphology of the secondary cell wall. In the schematic description of the secondary walls proposed by Boyd (1982), the fibrils oscillate around a principal direction, that we name direction 1, corresponding to the one defined by the MFA (Fig. 3a). Taking the case of perfectly aligned fibrils as a reference (Fig. 3b), we will examine the effect of fibrils oscillations (Fig. 3c). In this study, two different ways to describe these oscillations will be considered. In the first configuration, the fibrils are only allowed to oscillate within the plane (1, 2) while in the second configuration they can oscillate within both planes (1, 2) and (1, 3) (Fig. 3).

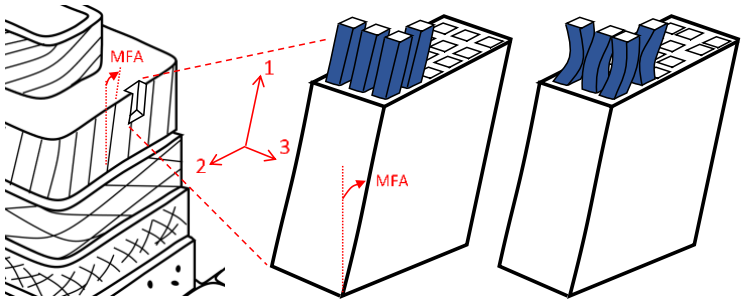

Fig. 3 Representation of the material constituting the secondary cell wall: **a** position and orientation of a portion of the cell wall, **b** classical representation with straight and parallel fibrils and **c** improved description with oscillated and connected fibrils.

2.1 Model of microstructure with one-directional oscillation

The first configuration, that we will call hereafter the microstructure (or model) 1S, consists of an assemblage of periodic cells, made of two connected cylindrical fibrils with a rectangular section which oscillate within the plane (1, 2) along the direction (1) as described by Fig. 4.

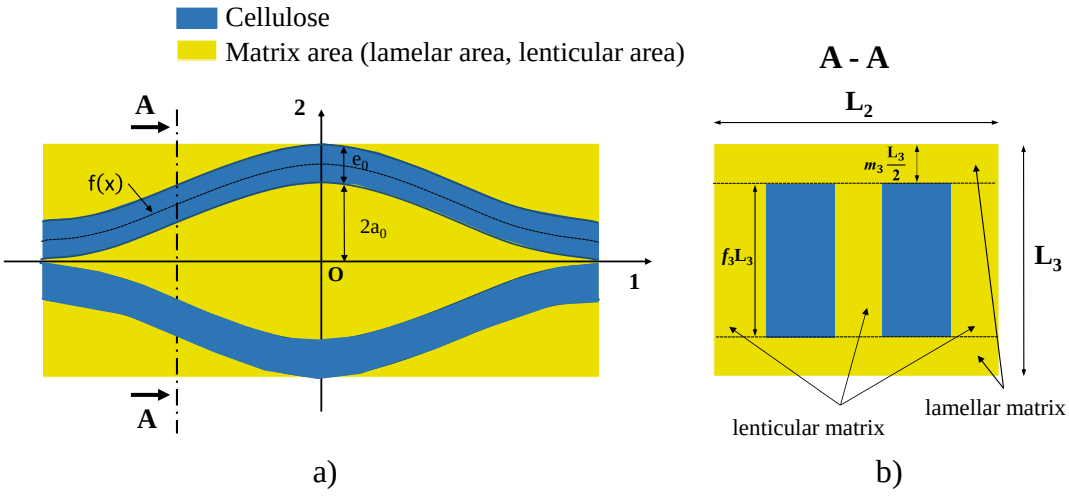

Fig. 4 Description of the periodic cell associated with microstructure 1S: (**a)** Cross-section of the periodic cell in the plane (1, 2) for z = 0 and; (**b)** cross-section A-A of the periodic cell in the plane (2, 3) (After Bonnet 2017).

The periodic cell is a rectangular parallelepiped of sides L_1, L_2, L_3, made of a lenticular layer surrounded by two lamellar coatings which are geometrically defined as follows.

The lenticular layer is a rectangular parallelepiped of sides L_1, L_2, f_3L_3 made of the two cylindrical fibrils of rectangular section which oscillate in the plane (1, 2) along the direction 1 and are connected at $x = \pm L_1/2$ - where x, y, z correspond to the coordinates in the direction 1, 2, 3, respectively. The f_3 parameter is defined such that f_3L_3 is the fibril width in direction 3 - which also corresponds to the local radial direction of the cell wall. Both fibrils are surrounded by a matrix which will be called the lenticular matrix in what follows. If we consider the cross-section z = 0 of the periodic cell, the oscillations of the fibrils are represented by sine curves in the plane (1, 2) (see Fig. 4a). For instance, the fibril in the upper part ($y > 0$) of the periodic cell is described by a function f(x) defined by.

$$f(x) = a_0 \cos\left(\frac{2\pi}{L_1}x\right) + a_0 + \frac{e_0}{2} \tag{1}$$

where L_1 and a_0 are respectively the period and amplitude of the sine curve and where e_0 is the fibril width in direction 2.

The lenticular layer is surrounded by two lamellar coatings which are only made of matrix. In what follows, the matrix in both lamellar coatings will be referred to as the lamellar matrix. It should be noted that the matrix of the lamellar coating and the one of the lenticular layer corresponds to the same material. Each lamellar coating is a rectangular parallelepiped of sides L_1, L_2, m_3L_3 with $m_3 = 1 - f_3$ and where, f_3 and m_3 stand for the linear proportion of fibrils and matrix in the direction 3, respectively. For later use, we define the parameter r_λ which corresponds to the ratio between the volume of lamellar matrix and the volume of lenticular matrix. Simple geometrical considerations show that

$$r_\lambda = \frac{V_{\text{lamellar matrix}}}{V_{\text{lenticular matrix}}} = \frac{1 - f_3}{f_3(1 - f_2)} \tag{2}$$

where f_2, similarly to f_3, is the linear proportion of fibrils in direction 2. Further, the volume fraction c of the fibrils is given by

$$c = f_2 f_3 \tag{3}$$

From the description of the periodic cell associated with the microstructure 1S, we can easily obtain the geometrical description of the periodic cell associated with a microstructure for which the fibrils are straight and parallel. Indeed, for such a microstructure - which will be called 0S in the sequel, the periodic cell is still made of a lenticular layer surrounded by two lamellar coatings. However, the lenticular layer is now composed of two cylindrical fibrils of rectangular section which are parallel to the direction 1 instead of oscillating around this direction as in microstructure 1S. During all this study, we make use of microstructure 0S as the reference solution to investigate the influence of the oscillations and connectedness of the fibrils on the effective cell wall behavior.

2.2 Model of microstructure with two-directional oscillations

In the microstructure (or model) 2S, the fibrils are allowed to oscillate in two directions, that is in the (1, 2) plane but also in the (1, 3) plane. The fibrils are assumed to be cylindrical with a square cross-section and to oscillate as a helix around the direction 1 (see Fig. 5a). The periodic elementary cell of microstructure 2S is now a rectangular parallelepiped of sides (L_1, 4ℓ, 4ℓ). It is composed of 4 rectangular parallelepipedic subdomains of sides (L_1, 2ℓ, 2ℓ) where each subdomain contains one helical fibril oscillating in both planes (1, 2) and (1, 3) (see Fig. 5b and Fig. 5c). Note that for each of the four subdomains, the point O_i follows the central axis of each helix, and the point C_i, located at the center of fiber i (for i = 1, ..., 4), winds up in helix around the axe (O_i, x). As each fibril makes a complete turn for each period L_1 in the direction x, the adjacent fibrils are in phase opposition. Accordingly, a fibril is connected with each of its neighbors one time per period L_1.

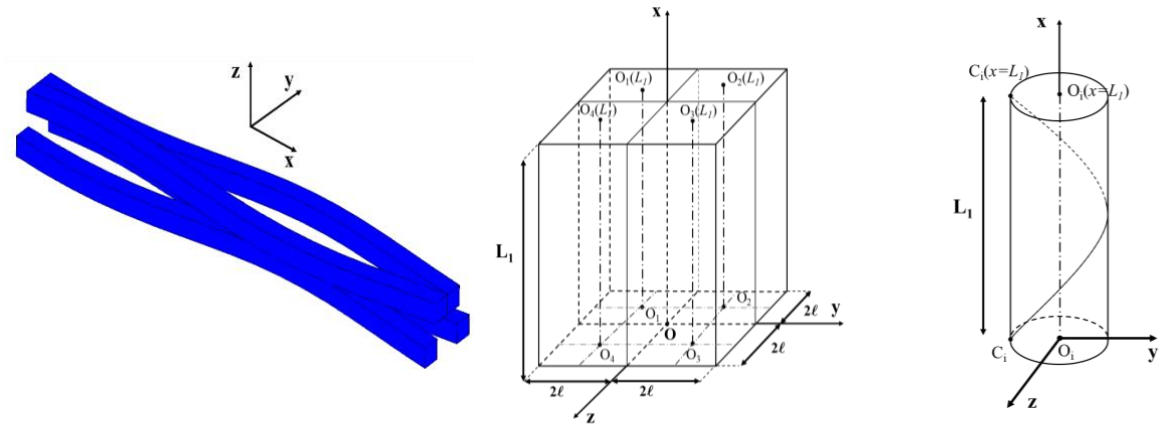

(a) (b) (c)

Fig. 5 Description of the periodic elementary cell associated with microstructure 2S: **a** Oscillations of the fibrils within the periodic cell, **b** Schematization of the 4 subdomains of the periodic elementary cell and **c** Helical path of a point C_i

Lastly, it should be noted that $m\ell$ stands for the radius of the cylinder in which the trajectory of each helix is located (see Fig. 5). The linear proportion of matrix is given by $m = 1 - f = 1 - \sqrt{c}$ since the linear proportion of fibrils f is equal to $\sqrt{c}$ for a fibril square cross-section of side $2f\ell$.

3 Computation of the effective behavior of the cell wall in the framework of linear elasticity

3.1 Local problem and effective behavior

In section 2, we defined 3 microstructure models (0S, 1S, and 2S) which approximate the real microstructure of the S2 cell wall. We now have to determine the effective elastic properties of the S2 cell wall associated with each of these periodic microstructures. For that, we make use of a deformation approach and apply to each periodic unit cell periodic boundary conditions of the type $\underline{u}(\underline{x}) = \underline{\underline{\varepsilon}}\,x + \underline{u}'(\underline{x})$ where $\underline{\underline{\varepsilon}}$ is the imposed macroscopic strain and $\underline{u}'(\underline{x})$ a periodic displacement field [19]. The local problem to be solved reads as follows:

$$\left.\begin{cases} \underline{div}\left(\underline{\underline{\sigma}}(\underline{x})\right) = 0 \\ \underline{\underline{\sigma}}(\underline{x}) = \underline{\underline{\underline{\underline{C}}}}(\underline{x}) : \underline{\underline{\varepsilon}}(\underline{x}) \\ \underline{\underline{\varepsilon}}(\underline{x}) = \dfrac{1}{2}\left(\dfrac{\partial \underline{u}(\underline{x})}{\partial(\underline{x})} + \dfrac{\partial \underline{u}(\underline{x})}{\partial(\underline{x})}^{T}\right) \end{cases}\right\} \forall x \in \Omega$$
$$u(\underline{x}) = \underline{\underline{\varepsilon}}\,x + u'(\underline{x}), \text{ with periodic } u', \forall x \in \partial\Omega \qquad (4)$$

where Ω stands for the RVE, i.e. the periodic unit cell, and $\partial\Omega$ the cell boundary. The fourth-order tensor $\underline{\underline{\underline{\underline{C}}}}(\underline{x})$ is given by $\underline{\underline{\underline{\underline{C}}}}(\underline{x}) = \sum_{r=M,F} \underline{\underline{\underline{\underline{C}}}}^{r}.\chi^{r}(x) = \underline{\underline{\underline{\underline{C}}}}^{M}.\chi^{M}(x) + \underline{\underline{\underline{\underline{C}}}}^{F}.\chi^{F}(x)$ where $\chi^{r}(x)$ is the characteristic function of the phase r, equal to 1 if $\underline{x}$ belongs to the phase r and zero otherwise. The tensor $\underline{\underline{\underline{\underline{C}}}}^{r}$ are the tensors of the elastic moduli of the phases $r = (M, F)$ where the subscript M and F stand for the matrix and the fibrils respectively. Furthermore, perfect interfaces are assumed between the matrix and the fibrils.

By applying 6 different elementary loadings to the periodic unit cell and solving by means of the FE method the local problem, we obtain for each elementary loading the local stress field, thus allowing us to determine the macroscopic stress which is classically defined by:

$$\underline{\underline{\overline{\sigma}}} = \langle \underline{\underline{\sigma}} \rangle = \frac{1}{|\mathrm{VER}|} \int_{\mathrm{VER}} \underline{\underline{\sigma}}(\underline{x}) d\underline{x} \tag{5}$$

The tensor of the effective elastic moduli $\tilde{\mathrm{C}}$ of the cell wall is then obtained by the following relation

$$\underline{\underline{\overline{\sigma}}} = \underline{\underline{\underline{\underline{\tilde{C}}}}} : \underline{\underline{\overline{\varepsilon}}} \tag{6}$$

which, by using Voigt notations, can be rewritten as

$$\underline{\underline{\overline{\sigma}}} = \underline{\underline{\underline{\underline{\tilde{C}}}}} : \underline{\underline{\overline{\varepsilon}}} \Leftrightarrow \begin{pmatrix} \overline{\sigma}_1 \\ \overline{\sigma}_2 \\ \overline{\sigma}_3 \\ \overline{\sigma}_4 \\ \overline{\sigma}_5 \\ \overline{\sigma}_6 \end{pmatrix} = \begin{pmatrix} \tilde{C}_{11} & \tilde{C}_{12} & \tilde{C}_{13} & \tilde{C}_{14} & \tilde{C}_{15} & \tilde{C}_{16} \\ \tilde{C}_{21} & \tilde{C}_{22} & \tilde{C}_{23} & \tilde{C}_{24} & \tilde{C}_{25} & \tilde{C}_{26} \\ \tilde{C}_{31} & \tilde{C}_{32} & \tilde{C}_{33} & \tilde{C}_{34} & \tilde{C}_{35} & \tilde{C}_{36} \\ \tilde{C}_{41} & \tilde{C}_{42} & \tilde{C}_{43} & \tilde{C}_{44} & \tilde{C}_{45} & \tilde{C}_{46} \\ \tilde{C}_{51} & \tilde{C}_{52} & \tilde{C}_{53} & \tilde{C}_{54} & \tilde{C}_{55} & \tilde{C}_{56} \\ \tilde{C}_{61} & \tilde{C}_{62} & \tilde{C}_{63} & \tilde{C}_{64} & \tilde{C}_{65} & \tilde{C}_{66} \end{pmatrix} \begin{pmatrix} \overline{\varepsilon}_1 \\ \overline{\varepsilon}_2 \\ \overline{\varepsilon}_3 \\ \overline{\varepsilon}_4 \\ \overline{\varepsilon}_5 \\ \overline{\varepsilon}_6 \end{pmatrix} \tag{7}$$

where $\overline{\sigma}_i = \overline{\sigma}_{ii}$, $\overline{\varepsilon}_i = \overline{\varepsilon}_{ii}$ for i = 1 à 3 and $\overline{\sigma}_4 = \overline{\sigma}_{23}$; $\overline{\sigma}_5 = \overline{\sigma}_{13}$; $\overline{\sigma}_6 = \overline{\sigma}_{12}$; $\overline{\varepsilon}_4 = 2\overline{\varepsilon}_{23}$; $\overline{\varepsilon}_5 = 2\overline{\varepsilon}_{13}$; $\overline{\varepsilon}_6 = 2\overline{\varepsilon}_{12}$

For instance, if we apply an elementary loading of the form $\underline{\underline{\overline{\varepsilon}}} = \underline{e}_1 \otimes \underline{e}_1$, the first column of the second-order tensor $\underline{\underline{\underline{\underline{\tilde{C}}}}}$ is given by:

$\tilde{C}_{11} = \overline{\sigma}_1 = \langle \sigma_{11} \rangle$; $\tilde{C}_{21} = \overline{\sigma}_2 = \langle \sigma_{22} \rangle$; $\tilde{C}_{31} = \overline{\sigma}_3 = \langle \sigma_{33} \rangle$; $\tilde{C}_{41} = \overline{\sigma}_4 = \langle \sigma_{23} \rangle$; $\tilde{C}_{51} = \overline{\sigma}_5 = \langle \sigma_{13} \rangle$; $\tilde{C}_{61} = \overline{\sigma}_6 = \langle \sigma_{12} \rangle$

Accordingly, the application of 6 independent elementary loadings provide the whole effective tensor $\underline{\underline{\underline{\underline{\tilde{C}}}}}$ of elastic moduli.

3.2 Mesh description

In order to analyze the influence of the fibrils oscillations on the effective behavior of the cell wall, FE calculations are carried out on the three periodic elementary cells presented in section 2 which correspond respectively to the model 0S, 1S and 2S. The volumetric meshes are generated by means of cubic elements with 8 nodes. As already mentioned, the fibrils-matrix interfaces are assumed to be perfect. A schematic description of the obtained meshes for each of the 3 microstructures is given in Fig. 6.

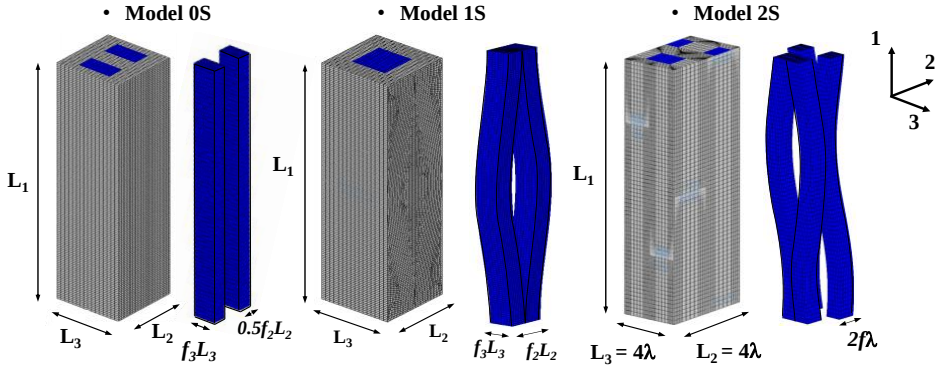

Fig. 6 Meshes of model 0S, 1S and 2S

3.3 Mechanical properties of the phases

In this study, relying on the work of Cave [4], we assume that the fibrils, which mainly consist of crystalline cellulose, are linear elastic and transversely isotropic. We denote by *L* the direction corresponding to the fibrils orientation and by *TT* the transverse plane in which the behavior is isotropic elastic. Accordingly, the compliance tensor of the fibrils is classically given by

$$\underline{\underline{S}}^F = \left(\underline{\underline{C}}^F\right)^{-1} = \begin{pmatrix} \frac{1}{E_L^F} & \frac{-\nu_{TL}^F}{E_T^F} & \frac{-\nu_{TL}^F}{E_T^F} & 0 & 0 & 0 \\ \frac{-\nu_{TL}^F}{E_T^F} & \frac{1}{E_T^F} & \frac{-\nu_{TT}^F}{E_T^F} & 0 & 0 & 0 \\ \frac{-\nu_{TL}^F}{E_T^F} & \frac{-\nu_{TT}^F}{E_T^F} & \frac{1}{E_T^F} & 0 & 0 & 0 \\ 0 & 0 & 0 & \frac{1}{G_{TT}^F} & 0 & 0 \\ 0 & 0 & 0 & 0 & \frac{1}{G_{LT}^F} & 0 \\ 0 & 0 & 0 & 0 & 0 & \frac{1}{G_{LT}^F} \end{pmatrix} \tag{8}$$

where E_L^F is the Young modulus in the fibrils direction, E_{TT}^F the Young modulus in the transverse plane, ν_{LT}^F and ν_{TT}^F the Poisson ratios in the planes LT and TT, G_{LT}^F and $G_{TT}^F = [E_T^F/2(1+\nu_{TT}^F)]$ the shear moduli in the plane LT and TT.

The matrix is made of the amorphous constituents of the wood that is mainly of lignin and hemicellulose. Based on the work of Tang and Hsu [20], the matrix behavior is assumed to be isotropic linear elastic with Young modulus E^M and Poisson ratio ν^M.

From the symmetry properties of both the geometrical shape of the unit cell and the behavior of the phases (isotropic matrix and transversely isotropic fibrils), we can deduce the symmetry properties of the effective behavior of the S2 cell wall when its microstructure is described either by the model 1S or the model 2S. Indeed, for the microstructure 1S, it is easy to note (see Fig. 4) that the plane (O, 1, 2) and (O, 1, 3), where O is the center of the unit cell, are two symmetry planes for the S2 cell wall. Accordingly, the linear effective elastic behavior of the cell wall for the microstructure 1S is orthotropic and reads

$$\begin{pmatrix} \bar{\sigma}_1 \\ \bar{\sigma}_2 \\ \bar{\sigma}_3 \\ \bar{\sigma}_4 \\ \bar{\sigma}_5 \\ \bar{\sigma}_6 \end{pmatrix} = \begin{pmatrix} \tilde{C}_{11} & \tilde{C}_{12} & \tilde{C}_{13} & 0 & 0 & 0 \\ \tilde{C}_{12} & \tilde{C}_{22} & \tilde{C}_{23} & 0 & 0 & 0 \\ \tilde{C}_{31} & \tilde{C}_{32} & \tilde{C}_{33} & 0 & 0 & 0 \\ 0 & 0 & 0 & \tilde{C}_{44} & 0 & 0 \\ 0 & 0 & 0 & 0 & \tilde{C}_{55} & 0 \\ 0 & 0 & 0 & 0 & 0 & \tilde{C}_{66} \end{pmatrix} \begin{pmatrix} \bar{\varepsilon}_1 \\ \bar{\varepsilon}_2 \\ \bar{\varepsilon}_3 \\ \bar{\varepsilon}_4 \\ \bar{\varepsilon}_5 \\ \bar{\varepsilon}_6 \end{pmatrix} \Leftrightarrow \begin{pmatrix} \bar{\varepsilon}_1 \\ \bar{\varepsilon}_2 \\ \bar{\varepsilon}_3 \\ \bar{\varepsilon}_4 \\ \bar{\varepsilon}_5 \\ \bar{\varepsilon}_6 \end{pmatrix} = \begin{pmatrix} \tilde{S}_{11} & \tilde{S}_{12} & \tilde{S}_{13} & 0 & 0 & 0 \\ \tilde{S}_{12} & \tilde{S}_{22} & \tilde{S}_{23} & 0 & 0 & 0 \\ \tilde{S}_{31} & \tilde{S}_{32} & \tilde{S}_{33} & 0 & 0 & 0 \\ 0 & 0 & 0 & \tilde{S}_{44} & 0 & 0 \\ 0 & 0 & 0 & 0 & \tilde{S}_{55} & 0 \\ 0 & 0 & 0 & 0 & 0 & \tilde{S}_{66} \end{pmatrix} \begin{pmatrix} \bar{\sigma}_1 \\ \bar{\sigma}_2 \\ \bar{\sigma}_3 \\ \bar{\sigma}_4 \\ \bar{\sigma}_5 \\ \bar{\sigma}_6 \end{pmatrix} \tag{9}$$

where the relations between the components of the tensor $\underline{\underline{\tilde{C}}}$ and $\underline{\underline{\tilde{S}}} = \underline{\underline{\tilde{C}}}^{-1}$ are recalled in Appendix A. Therefore, only 9 coefficients are required to characterize the effective elastic behavior associated with the model 1S. Note that the same reasoning can be applied to model 0S.

For the microstructure 2S, the derivation of the symmetry properties of the effective behavior is a bit more complicated. Let us first call a "central" symmetry the operation which transforms any point M of coordinates (x, y, z) by a point M' of coordinates (-x, -y, -z). If we apply to the periodic unit cell associated with the microstructure 2S first a plane symmetry (O, x, y) (see Fig. 5b for the definition of the direction x, y, z) and then a central symmetry, we notice that the microstructure 2S is invariant by such a transformation. Therefore, the tensor of moduli $\tilde{C}$ is also invariant by such a transformation. Moreover, any two-order (or fourth-order) tensor is invariant by a "central" symmetry. Accordingly, the tensor of moduli $\tilde{C}$ is also invariant by a central symmetry. Since the tensor of moduli $\underline{\underline{\tilde{C}}}$ is, on one hand, invariant for the combination of the plane symmetry (O, x, y) with the central symmetry, in the other hand, invariant for the central symmetry, it induces that it is also invariant for the plane symmetry (O, x, y). By applying the same argument with the plane symmetry (O, x, z), we infer that the tensor of moduli $\underline{\underline{\tilde{C}}}$ is also invariant for the plane symmetry (O, x, z). Therefore, the effective behavior is orthotropic. Lastly, noting that the microstructure 2S is also invariant by any rotation of angle π/2 around the direction (O*x*), it comes that the tensor of moduli $\underline{\underline{\tilde{C}}}$ is quadratic, that is orthotropic with two equivalent directions (O*y*) and (O*z*).

4 Application to model 1S

In this section, we analyze the influence of the fibrils oscillations when associated with the microstructure 1S. For that, we compute by means of the FE software Cast3M the effective behavior of the cell wall by making use of the methodology presented in Section 3.

4.1 Numerical accuracy

Firstly, we carry out a convergence study to determine the number of finite elements to be used in the following simulations. The geometrical parameters defining the periodic unit cell are given by Eq. (11) while the material parameters defining the behavior of the phases are provided in Table 2. The concentration of the fibrils is set to c = 50%. To analyze the convergence of the solution, we make use of the following difference parameter:

$$diff^{(i)} = \left[\frac{1}{N}\sum\left(\frac{\widetilde{C}_{kl}^{i} - \widetilde{C}_{kl}^{+\infty}}{\widetilde{C}_{kl}^{+\infty}}\right)^{2}\right]^{\frac{1}{2}} \tag{10}$$

where N is the number of components which differs from zero, i.e. 9 for an orthotropic behavior, $\widetilde{C}_{kl}^{i}$ the value of the component $\widetilde{C}_{kl}$ for the mesh number i, $\widetilde{C}_{kl}^{+\infty}$ the value of the component $\widetilde{C}_{kl}$ for the most refined mesh (542 400 Elements). The evolution of $diff^{(i)}$ as a function of the FE number is reported in Fig. 7. In order to impose an accuracy less than 1%, all the FE simulations associated with microstructure 1S (and also 0S) are carried out in this study with a mesh of 21 216 elements.

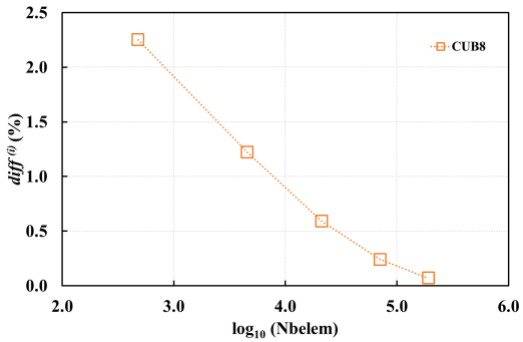

Fig. 7. Evolution of the difference parameter $diff^{(i)}$

4.2 Influence of the fibrils oscillations on the cell wall effective behavior

4.2.1 Reference solution

In order to analyze the influence of the fibrils oscillations on the effective behavior of the cell wall, we compare the different components of the effective behavior associated with microstructures 1S and 0S. For that, we carry out a parameter study by varying some parameters and keeping others fixed. To determine the values of the fixed parameters, we consider a reference solution that corresponds to realistic values of the geometrical and material parameters of the wood. To this end, we use results stemming from literature for the geometrical parameters L_1, L_2 and L_3. For that, the typically lateral dimensions of the wood fibrils are issued from the work of Salmén and Burgert [12]. Otherwise, concerning the axial direction of the fibrils, no direct data are available in the literature, but we can estimate, based on scanning electron microscope (SEM) photographs by Ruel [21] carried out on delignified wood by the white-rot fungus, the order of the distance between the contacts points between fibrils. Accordingly, these parameters are given by:

$$L_1 = 0.3\ 10^{-6}\,\text{m},\ L_2 = 0.04\ 10^{-6}\,\text{m},\ L_3 = 0.02\ 10^{-6}\,\text{m} \tag{11}$$

The volume fraction of the fibrils is obtained by the synthesis of Neagu [22] reported in Table 1.

Table 1 Volume fraction of the different constituents of the cell wall S2 (in %)

	Cellulose	Hemicellulose	Lignin
S2	50	27	23

In a first approximation, we assume that the fibrils are made of real cellulose (and not perfect cellulose as it is the case of the microfibrils), thus setting their concentration to c = 50%. Moreover, the value of the parameter r_λ, which is the ratio between the lamellar and lenticular parts of the matrix (see Eq. (1)) is arbitrarily set to 1. Once the values of c and r_λ are set, one can deduce the values of f_2 and f_3 by means of Eqs. (2) and (3), thus leading to $f_2 = 4c/3$ and f_3=3/4.

The values of the material parameters used for the reference solution are given in Table 2 which presents data issued from the literature when it is considered that the fibrils behave like an isotropic transverse elastic material and the matrix as a linear isotropic elastic one. These data have been determined either from experiments E, from molecular dynamic simulations MD or by making use of phenomenological models P.

Table 2 Mechanical properties of the different constituents of the cell wall S2

Constituent	Coefficient		Value	Method	Reference
Cellulose	Longitudinal Young modulus	$\mathbf{E_L}$ (GPa)	138	**E**	[23]
	Transverse Young modulus	$\mathbf{E_{TT}}$ (GPa)	27.2	**MD**	[24]
	Longitudinal Poisson ratio	$\mathbf{nu_{LT}}$	0.1	**P**	[25]
	Transverse Poisson ratio	$\mathbf{nu_{TT}}$	0.33	**P**	[25]
	Longitudinal shear modulus	$\mathbf{G_{LT}}$ (GPa)	4.4	**MD**	[24]
	Transverse shear modulus	$\mathbf{G_{TT}}$ (GPa)	E_{TT} / 2(1+nu_{TT})	-	-
Amorphous matrix	Young modulus	$\mathbf{E_m}$ (GPa)	2	**E**	[26]
	Poisson ratio	$\boldsymbol{\upsilon_m}$	0.33	**E**	[27]

4.2.2 Variation of geometrical parameters

In this section, we analyze the influence of three geometrical parameters, that is the ratio r_λ, the shape parameter $r_\varphi = L_1/L_2$ and the fibrils volume fraction c, on the effective behavior of the cell wall. Four different values of the shape parameter r_φ (3.75, 7, 15, 30) will be considered for the model 1S and only one value for the model 0S since for trivial geometrical reason the values of $\widetilde{C}_{kl}$ for this microstructure does not depends on the shape ratio r_φ, and three values of r_λ (1/400, 1, 400). The third geometrical parameter, i.e. the volume fraction c, will be fixed to its reference value c = 0.5. To visualize the range of geometrical variations, some cases of r_φ and r_λ values are illustrated in Fig. 8.

Values of r_λ	$r_\varphi = \frac{L_1}{L_2} = 3.75$	$r_\varphi = \frac{L_1}{L_2} = 30$
$r_\lambda = \frac{1}{400}$	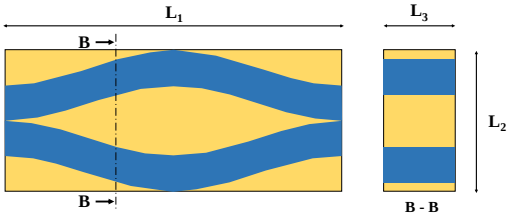	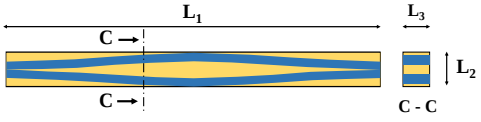

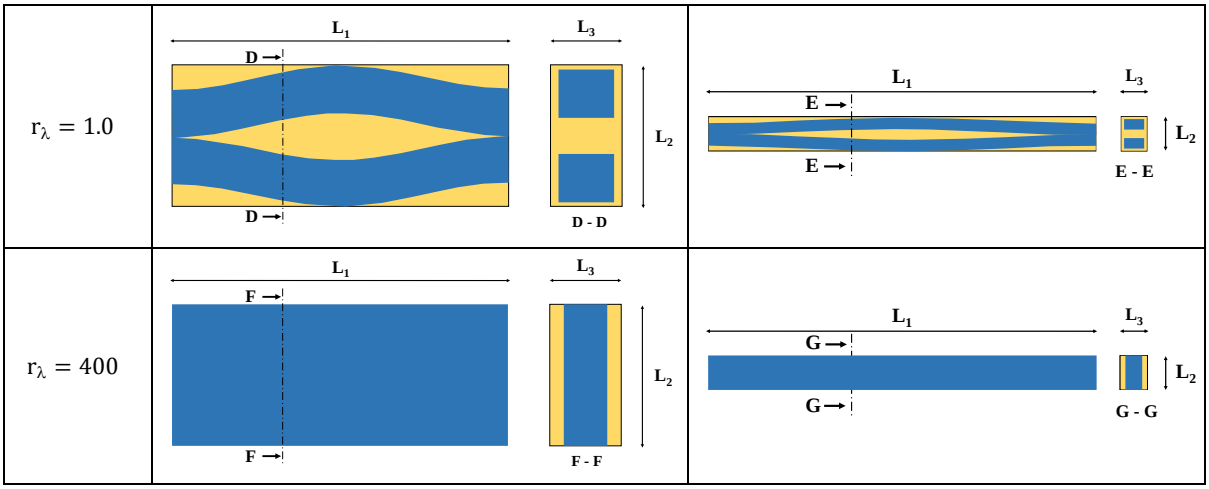

Fig. 8 : Illustration of the unit-cell geometry for different values of r_λ and r_φ (in connection with Fig. 9)

In Fig. 9, we reported the evolutions of the 9 elastic effective moduli which characterize the orthotropic elastic behavior of the cell wall S2 for the microstructures 0S and 1S as function of the ratio r_λ.

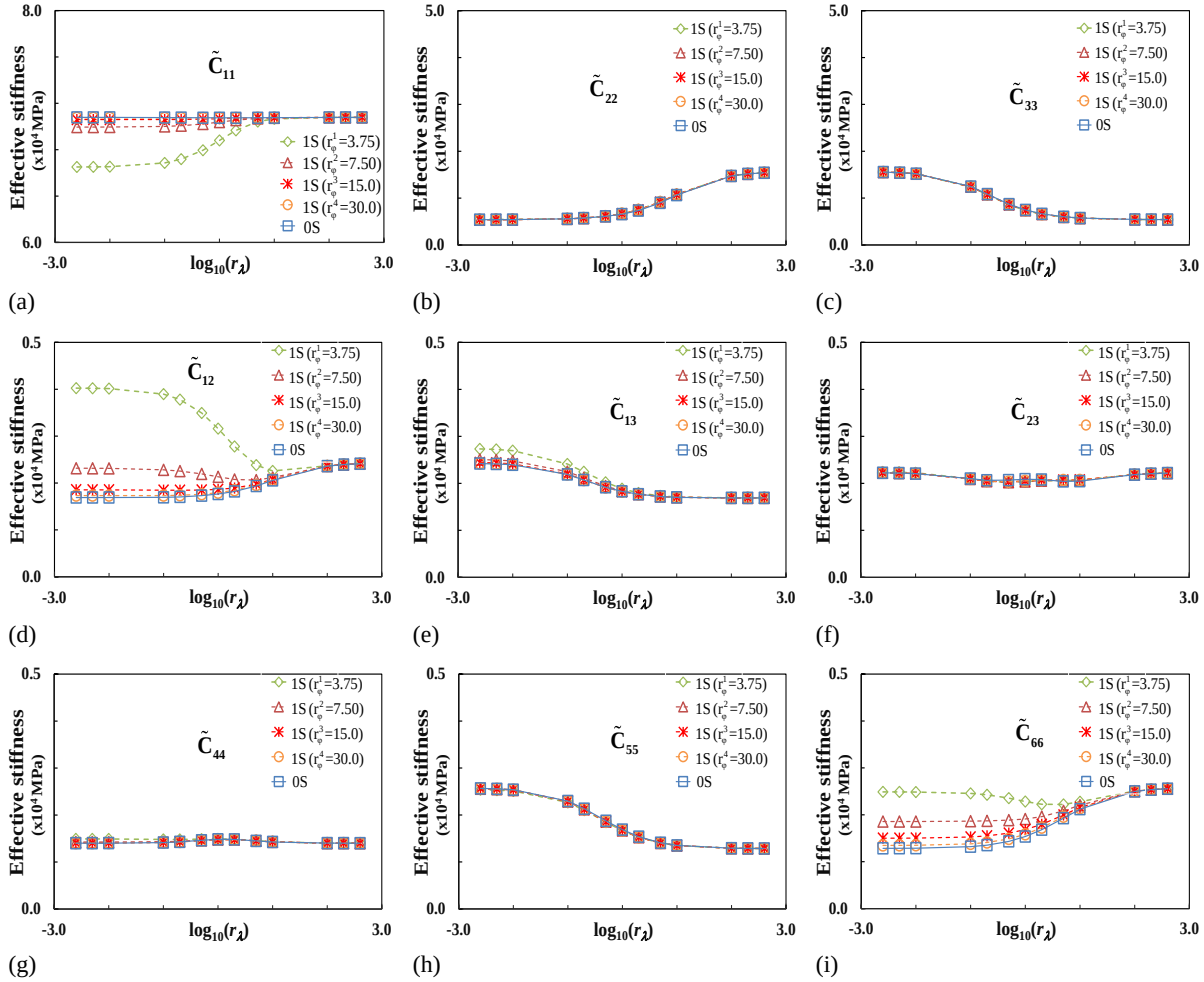

Fig. 9 Variations of the effective moduli $\widetilde{C}_{kl}$ of the cell wall as function of r_λ (c = 0.5)

We first observe that any component $\widetilde{C}_{kl}$ associated with the 1S model converges towards a value independent of r_φ when r_λ goes to $+\infty$. This is quite normal since the microstructures 1S and 0S converge towards a same two layers laminate when r_λ goes to $+\infty$. Then, we notice that only 2 components of the effective moduli, $\widetilde{C}_{12}$

and $\widetilde{C}_{66} = \widetilde{G}_{12}$, are strongly influenced by the oscillations of the fibrils. For the other moduli, the fibrils oscillations have a weak effect - for $\widetilde{C}_{11}, \widetilde{C}_{13}, \widetilde{C}_{44}$ - or even no effect at all - for $\widetilde{C}_{22}, \widetilde{C}_{33}, \widetilde{C}_{23}, \widetilde{C}_{55}$ - on the effective behavior of the cell wall.

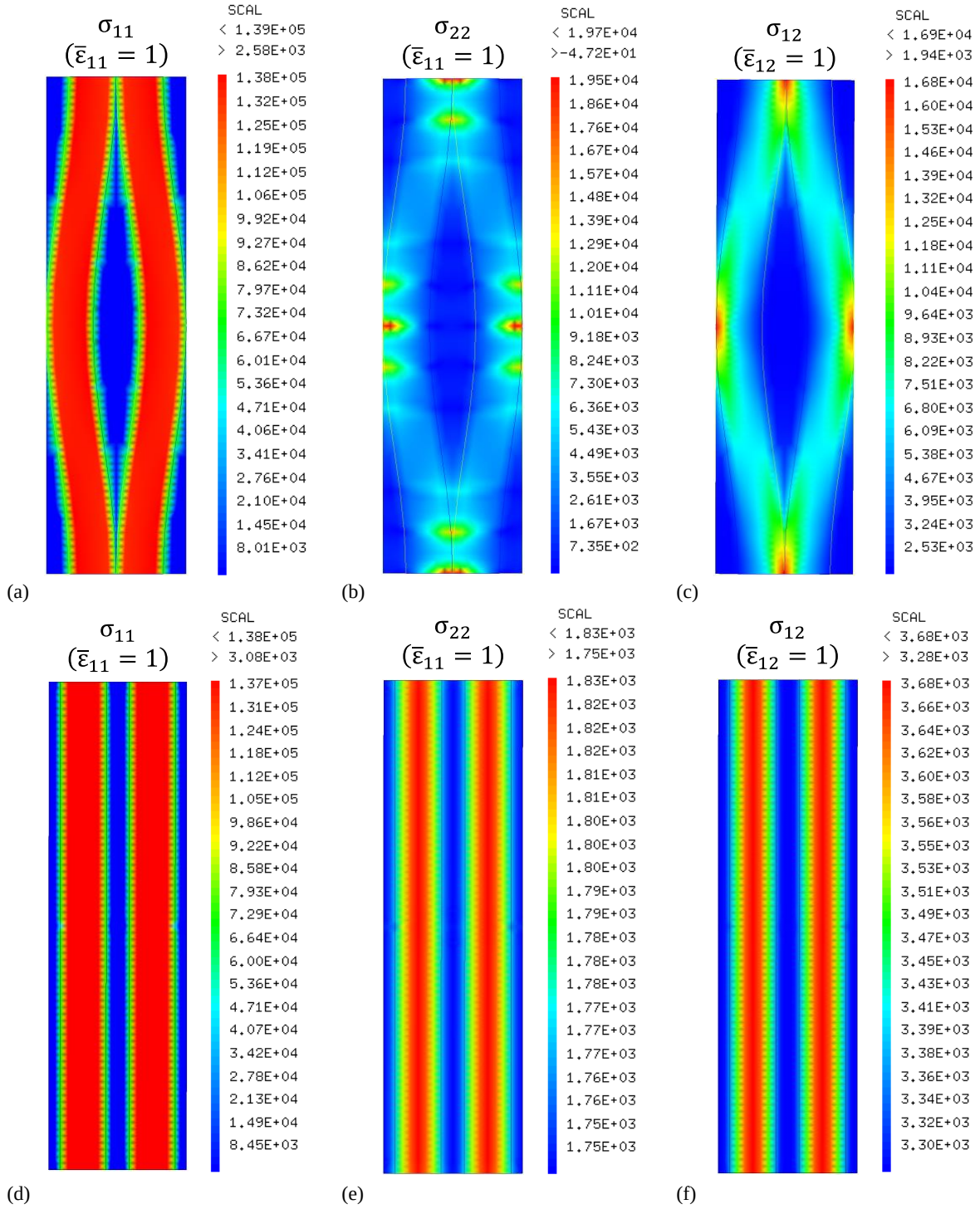

Fig. 10 Maps of selected components of the stress field in the plane (1, 2) obtained by FE calculations for two macroscopic loadings for both models 0S and 1S ($r_\varphi = 3.75$; $r_\lambda = 1.0$). Maps of σ_{11} for $\overline{\varepsilon}_{11} = 1$: (a) model 1S, (d) model 0S. Maps of σ_{22} for $\overline{\varepsilon}_{11} = 1$: (b) model 1S, (e) model 0S. Maps of σ_{12} for $\overline{\varepsilon}_{12} = 1$: (c) model 1S, (f) model 0S.

To explain why only $\widetilde{C}_{66} = \widetilde{G}_{12}$ and $\widetilde{C}_{12}$ are strongly influenced by the oscillations of the fibrils, we report some selected component of the stress field in Fig. 10 for the reference values $r_\lambda = 1$ and $r_\varphi = 3.75$. In a first time, we compare for both models 1S (Fig. 10c) and 0S (Fig. 10f) the component σ_{12} of the stress field in the plane (1,2) - namely z = 0 - obtained by FE calculations for a macroscopic loading defined by $\overline{\varepsilon}_{12} = 1$ and $\overline{\varepsilon}_{ij} = 0$

for the other components. It should be noted that the spatial average of this field provides the effective coefficient $\widetilde{C}_{66}$. It is observed that both stress fields σ_{12}, associated with models 1S and 0S respectively, are significantly different, thus explaining why the effective modulus $\widetilde{C}_{66}$ is strongly influenced by the fibrils oscillations. Furthermore, the fibrils oscillations act as reinforcement for this modulus since, as observed in Fig. 10c and Fig. 10f, the stress field σ_{12} is significantly higher, particularly within the fibrils, for the model 1S than for 0S. The same explanation holds true for the effective modulus $\widetilde{C}_{12}$ which corresponds to the spatial average of the stress field σ_{22} obtained by FE calculations for a macroscopic loading defined by $\overline{\varepsilon}_{11} = 1$ and $\overline{\varepsilon}_{ij} = 0$ for the other components. By comparing this field in the plane (1, 2) for both models 1S (Fig. 10b) and 0S (Fig. 10e), it is again observed that both fields are significantly different and therefore lead to different values of $\widetilde{C}_{12}$ for both model 1S and 0S.

To explain why no (or no weak) effects of the fibrils oscillations are observed for the 7 remaining effective moduli $\widetilde{C}_{ij}$, we make use of the same type of comparison on the appropriate local stress field whose spatial average provides the considered effective modulus. For the sake of brevity, we only handle here the case of $\widetilde{C}_{11}$ but the argument is still valid for the remaining other moduli. By noticing that $\widetilde{C}_{11}$ corresponds to the spatial average of the component σ_{11} of the stress field obtained by FE calculations for a macroscopic loading defined by $\overline{\varepsilon}_{11} = 1$ and $\overline{\varepsilon}_{ij} = 0$ for the other components, we compare the values of this field in the plane (1, 2) for the models 1S (see Fig. 10a) and 0S (see Fig. 10d). It is observed that, unlike the cases we have dealt with so far, both stress fields σ_{11} associated with the models 1S and 0S respectively, are now close to each other (but not merged), thus explaining why a small but non zero effect of oscillating fibrils is observed for the coefficient $\widetilde{C}_{11}$.

Moreover, another argument helps to understand why the fibrils oscillations have a weak influence on the effective coefficient $\widetilde{C}_{11}$. For that, we make use of the slope p of the fibrils relative to direction 1 which is defined (see Eq. (1)) by

$$p = \frac{df(x)}{dx} = -a_0 \sin\left(\frac{2\pi x}{L_1}\right) \tag{12}$$

A straightforward calculation provides its mean value along the direction 1 as

$$\langle p \rangle = \frac{2}{r_\varphi}\left(\frac{1-c}{1+cr_\lambda}\right) \tag{13}$$

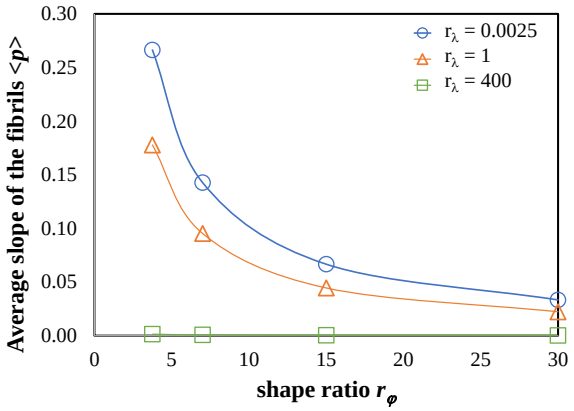

Fig. 11 : Variations of the average slope of the fibrils as a function of the shape factor r_φ for different values of r_λ (1S model)

The variations of the slope average <p> as function of the shape factor r_φ are displayed in Fig. 11. It is observed that its values are relatively weak – less than 18 % for all values of r_φ at the reference value $r_\lambda = 1$. Accordingly, for the longitudinal direction, the geometry of the model 1S is close to the one of the model 0S thus explaining why the variations of the effective modulus $\widetilde{C}_{11}$ for both model 1S and 0S are close to each other.

As the shape ratio which approximate the real oscillations of the cell wall is close to $r_\varphi = 7.5$, we report in Fig. 12 for this reference value the evolutions of the 9 engineering effective coefficients with respect to the ratio r_λ. For

that, we make use of Table 4 in Appendix A to compute their values from the knowledge of the elastic moduli $\widetilde{C}_{kl}$. It is observed that only 2 coefficients $\widetilde{G}_{12}, \tilde{\nu}_{12}$ are significantly influenced by the fibrils oscillations.

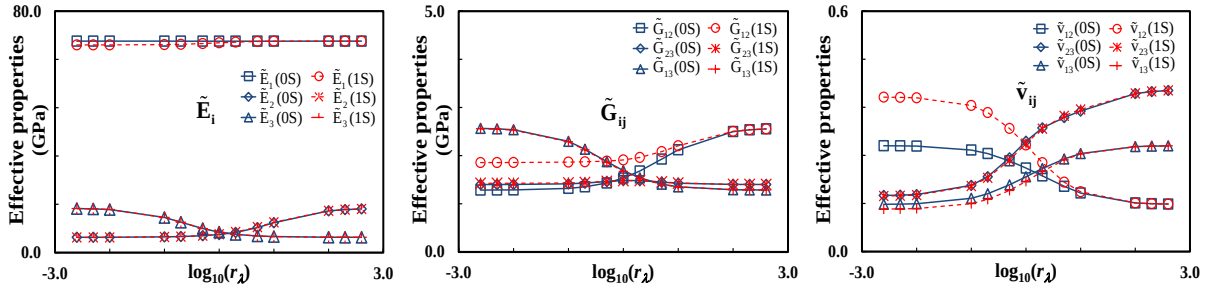

Fig. 12 Variations of the 9 engineering elastic coefficients characterizing the effective orthotropic behavior of the cell wall (r_φ = 7.5, c = 0.5)

We now analyze the evolutions, as function of the concentration, of the effective elastic moduli $\widetilde{C}_{kl}$ associated with both models of microstructure 1S and 0S for different values of the shape ratio r_φ at $r_\lambda = 1$. Again, it is observed that only the moduli $\widetilde{C}_{12}$ and $\widetilde{C}_{66} = \widetilde{G}_{12}$ are influenced by the fibrils oscillations (see Fig. 13). For the other moduli, not reported in this paper for the sake of concision, both microstructures 1S and 0S lead to the same results.

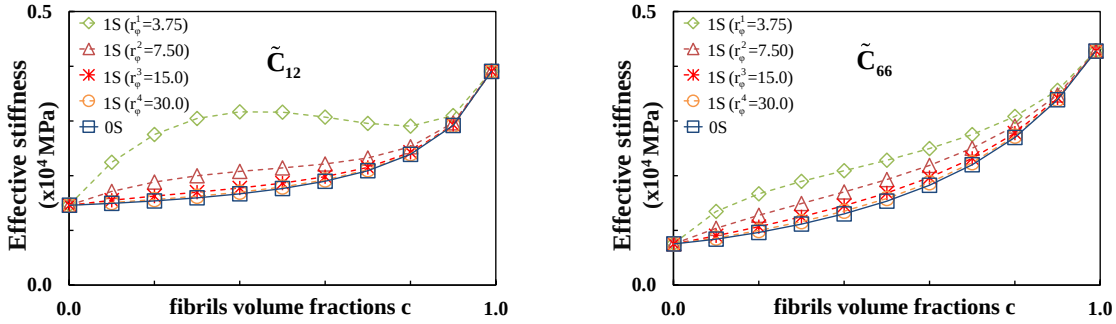

Fig. 13 Variations of the effective moduli $\widetilde{C}_{12}$ and $\widetilde{C}_{66}$ as function of the fibrils volume fraction (r_λ = 1)

Likewise, if we report the evolutions of the 9 engineering effective coefficients as function of the volume fraction, it is again observed that only both coefficients $\widetilde{G}_{12}, \tilde{\nu}_{12}$ are significantly influenced by the fibrils oscillations. In order to accurately characterize the sensibility of $\widetilde{G}_{12}, \tilde{\nu}_{12}$ to the fibers oscillations, we plotted in Fig. 14 their relative difference $\frac{\Delta\tilde{x}}{\tilde{x}^{0S}} = \left(\frac{\tilde{x}^{0S} - \tilde{x}^{1S}}{\tilde{x}^{0S}}\right)$ as function of the shape ratio r_φ for different values of the concentration. When $r_\varphi \leq 15.0$, it is observed that the relative differences $\Delta\widetilde{G}_{12}/\widetilde{G}_{12}^{0S}, \Delta\tilde{\nu}_{12}/\tilde{\nu}_{12}^{0S}$ remain significant whatever the value of the fibrils volume fraction.

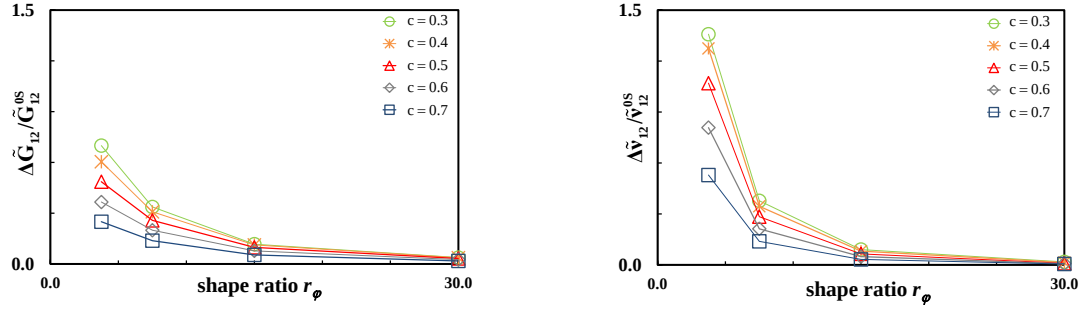

Fig. 14. Evolutions of the relative differences $\Delta\widetilde{G}_{12}/\widetilde{G}_{12}^{0S}, \Delta\tilde{\nu}_{12}/\tilde{\nu}_{12}^{0S}$ between the model 1S and 0S as functions of the shape ratio r_φ (r_λ = 1)

4.2.3 Variation of material parameters

In this section, we analyze the influence of the elastic contrast between the fibrils and the matrix, defined by the ratio E_L^F/E^M, on the effective properties of the cell wall. To this end, we compute the evolutions of the elastic engineering effective coefficients as functions of the shape ratio r_φ for different values of the elastic contrast. For that, we varied the value of the matrix Young modulus E^M from $E^M = E_L^F$ to $E^M = 10^{-2}E_L^F$ while keeping all the values of the fibrils material parameters fixed. The fibrils volume fraction and the ratio r_λ are set to their reference values, i.e. c = 0.5 and r_λ = 1.0. For the sake of concision, we only report the evolutions of the effective engineering coefficients which are significantly influenced by the fibrils oscillations, that is $\tilde{G}_{12}$ and $\tilde{\nu}_{12}$ again. In order to accurately characterize the sensibility of $\tilde{G}_{12}, \tilde{\nu}_{12}$ to the fibers oscillations, we have plotted in Fig. 15 their relative differences $\Delta\tilde{x}/\tilde{x}^{0S}$.

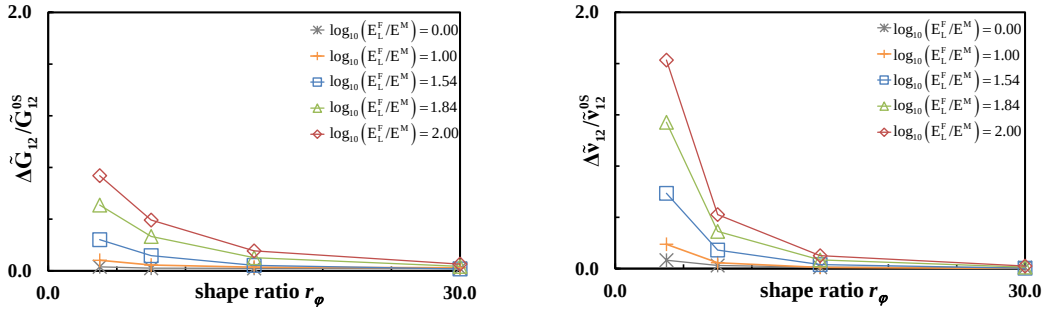

Fig. 15 Evolution of the relative differences $\Delta\tilde{G}_{12}/\tilde{G}_{12}^{0S}, \Delta\tilde{\nu}_{12}/\tilde{\nu}_{12}^{0S}$ between the models 1S and 0S for different values of the elastic contrast E_L^F/E^M (r_λ = 1 ; c = 0.5)

As expected, we observe in Fig. 15 that the influence of the fibers oscillations increases very significantly with the contrast. Note that the reference value of the contrast, which has been used in all the computations carried out in the former section, corresponds to $\log_{10}(E_L^F/E^M) = 1.84$.

5 Application to model 2S

In this section, we analyze the effects of the fibrils oscillations when described by microstructure 2S.

5.1 Numerical accuracy

Similarly to the model 1S, we first perform a convergence study to determine the number of finite elements to be used when carrying out FE simulations associated with microstructure 2S. For that, we still make use of the difference parameter $diff^{(i)}$ defined by Eq. (10) for which the most refined mesh is now made of 106 496 elements. We choose to impose an accuracy of 1.5% on the difference parameter which corresponds to a mesh of 14 976 elements.

5.2 Evaluation of the ratio r_λ

In order to compare the effective moduli obtained for each of the three microstructures 0S, 1S and 2S, we have to evaluate the value r_λ, used by models 0S and 1S, for which the results obtained for the model 2S are as close as possible to the ones obtained by models 1S and 0S. For that, we compute the relative gap $f(r_\lambda^i)$ between the effective moduli of models 2S and 1S for different values of the parameter r_λ. The relative gap is defined by

$$f(r_\lambda^i) = \left[\frac{1}{9}\sum\left(\frac{\tilde{C}_{kl}^{2S} - \tilde{C}_{kl}^{1S}(r_\lambda^i)}{\tilde{C}_{kl}^{2S}}\right)^2\right]^{\frac{1}{2}} \tag{14}$$

where the number 9 corresponds to the non-zero effective moduli $\tilde{C}_{kl}$ for an orthotropic elastic behavior, $\tilde{C}_{kl}^{1S}(r_\lambda^i)$ the values of the effective moduli associated with the microstructure 1S for a value r_λ^i and $\tilde{C}_{kl}^{2S}$ the values of the

effective moduli for the model 2S. In Fig. 16, we reported the evolutions of the relative gap as function of r_λ for different values of the volume fraction. It is observed that the relative gap reaches its minimum value for r_λ =1.

Accordingly, the value r_λ = 1 is used in all the comparisons performed in the sequel between the model 2S and the models 1S and 0S. It is worth noting that the obtained minimizing value r_λ = 1 coincidently corresponds to the reference value used in the parameter study carried out in Section 4, thus suggesting that it corresponds to a balanced contribution between the lamellar and lenticular matrix within the cell wall when described by the microstructure 1S.

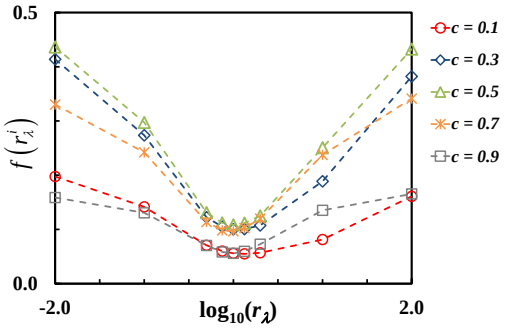

Fig. 16 Variation of the relative gap with respect to r_λ for different values of the volume fraction (r_φ = 7.5)

5.3 Influence of the fibrils oscillations on the cell wall effective behavior

Similarly to section 4, we carried out a parameter study by making vary different parameters such as the concentration, the shape ratio r_φ and the elastic contrast between the phases. In Fig. 17, we report the evolutions of the effective moduli $\widetilde{C}_{kl}$ for both models 0S and 2S as functions of the volume fraction for different values of the shape parameter r_φ. However, note that the variations of the effective moduli $\widetilde{C}_{11}$, $\widetilde{C}_{22}$, $\widetilde{C}_{33}$ are not reported since, as it was the case of the model 1S, they are not influenced by the oscillations of the fibrils, i.e. models 0S, 1S and 2S provide the same results.

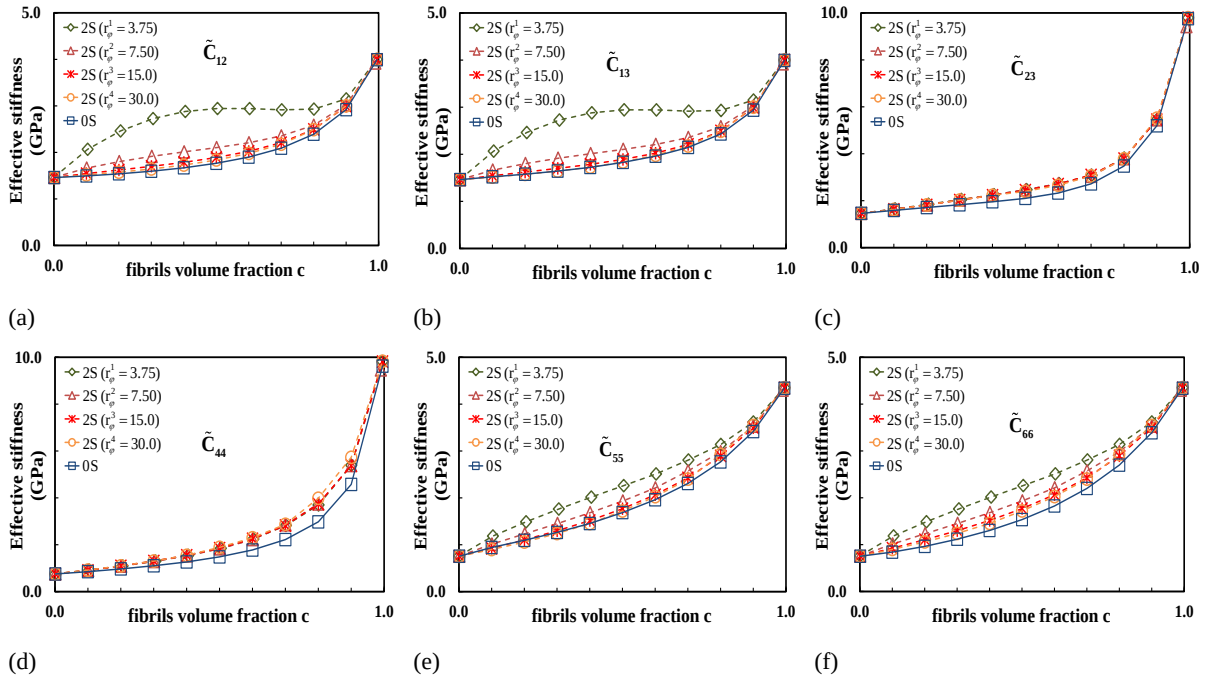

Fig. 17 Variations of the effective moduli $\widetilde{C}_{ij}$ as functions of the volume fraction (r_λ = 1)

We observe that the effect of the fibrils oscillations when described by the morphology 2S is quite significant not only on the effective moduli $\widetilde{C}_{12}$ and $\widetilde{C}_{66}$, as it was the case for the morphology 1S, but also on the moduli $\widetilde{C}_{13}$ and $\widetilde{C}_{55}$ whose values are the same as $\widetilde{C}_{12}$ and $\widetilde{C}_{66}$ for the model 2S. Such an effect was predictable since the fibrils for the morphology 2S are now in contact, in an equivalent way, both in the planes (1, 2) and (1, 3). Furthermore, the influence of fibrils oscillations is more pronounced for $\widetilde{C}_{12}$ and $\widetilde{C}_{13}$ than for $\widetilde{C}_{55}$ and $\widetilde{C}_{66}$, thus showing the existence of strong interactions between the longitudinal and transverse directions.

It is also observed that the effective moduli $\widetilde{C}_{23}$, $\widetilde{C}_{44}$ are slightly higher for the model 2S than for the model 0S, even for high values of the ratio r_φ. This last result was not expected. Indeed, intuitively one might expect that the effective properties associated with models 2S and 1S tend to the ones associated with the model 0S when r_φ tends to infinity since, in this situation, the fibrils tends to be parallel to the direction 1, as the model 0S. This is not always the case for the following reason. In fact, there is three effects induced by the fibrils oscillations. The first one is due to the orientation of the fibrils which ceases to be parallel to the direction 1. The second one stems from the contact between the fibrils. Lastly, the third one is induced by a heterogeneous spatial distribution of the matrix between the oscillating fibrils. When the ratio r_φ tends to infinity, the first two effects disappear since, in the one hand, the fibrils tend to have the same orientation as the direction 1, and in the other hand, the fibrils contact number by unit length tends to zero. However, the heterogeneous spatial distribution of the matrix between the oscillating fibrils, is still present even for high values of r_φ, thus explaining while the results derived by both models 2S and 1S can be different for some moduli to the ones associated with model 0S. Such an effect is observed for the model 2S on the effective moduli $\widetilde{C}_{23}$, $\widetilde{C}_{44}$ and also for $\widetilde{C}_{66}$. Note that this effect was already slightly noticeable for the model 1S on the effective moduli $\widetilde{G}_{12}$ (see Fig. 14) since the relative difference $\Delta\widetilde{G}_{12}/\widetilde{G}_{12}^{0S}$ does not tend to zero even for high values of r_φ - note that simulations carried out for r_φ = 120 give the same results than r_φ = 30. Lastly, it should be noted that the model 2S is quadratic – directions 2 and 3 are equivalent - contrary to the model 0S (and also 1S) which is, as numerically noticed, slightly orthotropic. Accordingly, effective coefficients implying equivalently directions 2 and 3, such $\widetilde{C}_{55}$ and $\widetilde{C}_{66}$, cannot be exactly the same for both models 2S and 0S for large values of r_φ.

Maps of selected components of the local mechanical fields like in Fig. 10 cannot be easily drawn for model 2S due to the complex 3D morphology of the fibrils. Instead, Table 3 gives the relative contribution of the fibrils to the calculation of each effective modulus $\widetilde{C}_{ij}$, calculated as the sum of the stress component concerned in the volume occupied by the fibrils, divided by the sum in the whole volume. The values for 01, 1S and 2S are given for comparison.

Table 3 Contribution of the fibrils to each effective modulus $\widetilde{C}_{ij}$ (in %)

ij	**11**	**22**	**33**	**23**	**13**	**12**	**44**	**55**	**66**
0S	97.80	60.53	65.72	38.22	30.87	7.26	52.91	66.57	61.43
1S	97.76	61.43	65.53	36.20	33.04	29.27	53.55	65.95	77.91
2S	97.79	63.55	63.55	48.87	57.79	24.62	64.30	77.83	77.83

The differences observed in Table 3 between the models 1S or 2S and 0S confirm the trends noted previously in Fig. 17. Note that for 2S the slope of the fibrils relative to direction 1 is constant and given by $\pi\left(1-\sqrt{c}\right)/\left(2r_\varphi\right)$; for c=0.5 and $r_\varphi = 3.75$ it is around 12%.

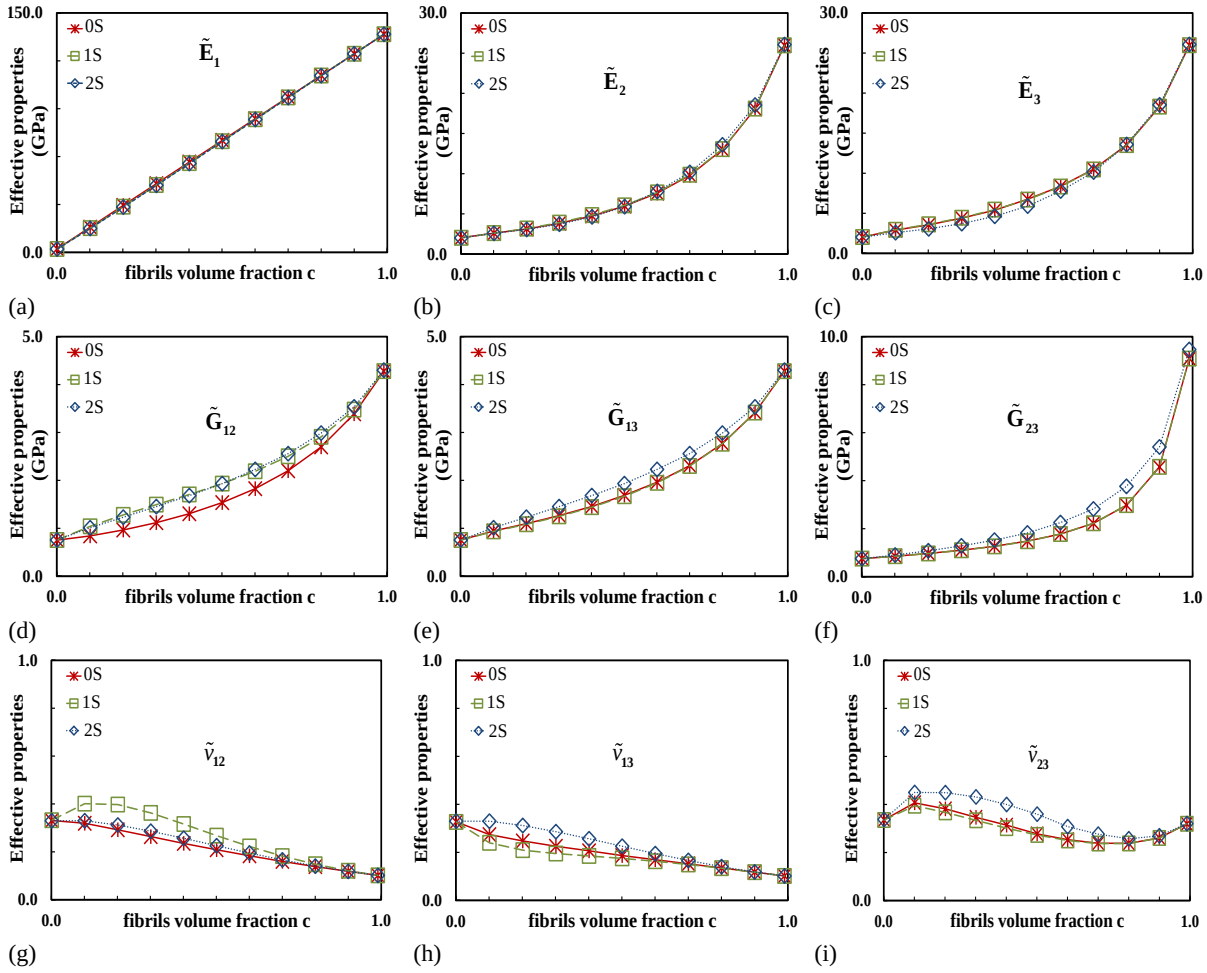

Fig. 18 Variations of the effective engineering coefficients as functions of the fibrils volume fraction ($r_\lambda = 1$, $r_\varphi = 7.5$)

If we now compare for the three models the variations of the engineering effective coefficients as functions of the volume fraction for a shape ratio set to its reference value $r_\varphi = 7.5$, it is again observed (see Fig. 18) that the evolutions of the Young effective moduli $\widetilde{E}_1$, $\widetilde{E}_2$, $\widetilde{E}_3$ are not influenced by the fibrils oscillations. As expected, $\widetilde{G}_{12} = \widetilde{C}_{66}$ is strongly influenced by the fibrils oscillations for both models 1S and 2S. Furthermore, its evolution is similar for both microstructures 1S and 2S. Surprisingly, this is not the case for the Poisson ratio $\tilde{\nu}_{12}$ for which the influence of the fibrils oscillations is rather weak when associated with model 2S. As expected again and unlike the model 1S, the fibers oscillations as described by the model 2S have a significant influence on the evolution of the shear modulus $\widetilde{G}_{13} = \widetilde{C}_{55}$ and Poisson ration $\tilde{\nu}_{13}$. Eventually, it is also observed for the model 2S, but not for the model 1S, a significant effect of the fibers oscillations on the effective coefficients $\widetilde{G}_{23} = \widetilde{C}_{44}$ and $\tilde{\nu}_{23}$.

Lastly, we reported for the three models in Fig. 19 the evolutions of the engineering effective coefficients - only the ones influenced by the fibril oscillations - as functions of the elastic contrast E_L^F/E^M, by making vary the matrix Young modulus and keeping the values of the other material parameters fixed. First, it is observed that for a limited contrast, i.e. $\log_{10}(E_L^F/E^M) \leq 1.5$, the fibrils oscillations have quite no influence on the effective behavior. However, for significant contrast, i.e. $\log_{10}(E_L^F/E^M) \geq 1.5$, the fibrils oscillations associated with the microstructure 2S have a significant effect on the effective coefficients $\widetilde{G}_{12}$, $\widetilde{G}_{13}$, $\tilde{\nu}_{12}$, $\tilde{\nu}_{13}$. Again, the evolutions of the shear modulus $\widetilde{G}_{12}$ are quite similar for both microstructure 2S and 1S while $\widetilde{G}_{13}$ and $\tilde{\nu}_{13}$, are only influenced by the fibril oscillations when associated with model 2S. Lastly, as observed in Fig. 19d, the influence of the fibrils oscillations on the effective Poisson ratio $\tilde{\nu}_{12}$ are stronger for the model 1S than for the model 2S.

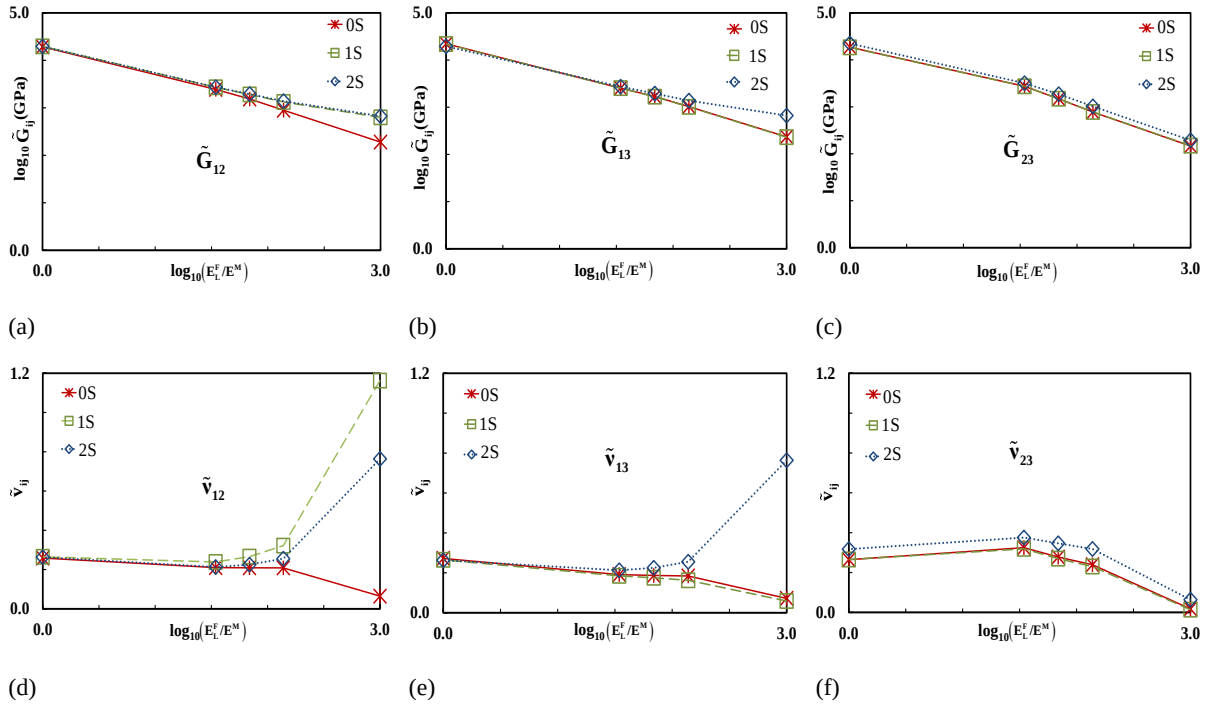

Fig. 19 Evolutions of the effective engineering coefficients as function of the elastic contrast (r_λ = 1, r_φ = 7.5 and c = 0.5)

6 Extension to hygro-mechanical behavior

This section aims at analyzing the influence of the fibril oscillations - when described by both microstructures 1S and 2S - on the effective strain induced by an increase (resp. a decrease) of the water content when no mechanical loading is applied. For that, we extend the numerical homogenization procedure presented in Section 2 to the case of linear hygro-elastic phases.

6.1 Computation of the effective behavior

The local problem to be solved is still described by Eq. (4) but now by replacing the constitutive elastic equations of the phases $(4)_2$ by the following one

$$\underline{\underline{\sigma}}(\underline{x}) = \underline{\underline{\underline{\underline{C}}}}(\underline{x}) : \underline{\underline{\varepsilon}}^{e}(\underline{x}) = \underline{\underline{\underline{\underline{C}}}}(\underline{x}) : \left(\underline{\underline{\varepsilon}}(\underline{x}) - \underline{\underline{\varepsilon}}^{\text{hygro}}(\underline{x})\right) \tag{15}$$

which describes a linear hygro-elastic behavior. In Eq. (15), $\underline{\underline{\varepsilon}}^{e}$ denotes the elastic strain, while $\underline{\underline{\varepsilon}}^{\text{hygro}}(\underline{x})$, which is the hydric strain, can be derived by the following constitutive relation

$$\underline{\underline{\varepsilon}}^{hygro}(x) = \underline{\underline{\alpha}}(x)\Delta h \tag{16}$$

where $\underline{\underline{\alpha}}(x)$ is the second-order hygro-expansion tensor and Δh the ambient humidity variation. The theory of homogenization shows that the effective behavior associated with such a local problem is itself linear hygro-elastic and therefore reads as

$$\overline{\underline{\sigma}} = \underline{\underline{\underline{\underline{\widetilde{C}}}}} : \left(\overline{\underline{\varepsilon}} - \overline{\underline{\varepsilon}}^{\text{hygro}}\right) = \underline{\underline{\underline{\underline{\widetilde{C}}}}} : \left(\overline{\underline{\varepsilon}} - \underline{\underline{\tilde{\alpha}}}\Delta h\right) = \underline{\underline{\underline{\underline{\widetilde{C}}}}} : \overline{\underline{\varepsilon}} + \underline{\tilde{\beta}} \tag{17}$$

where the second-order tensors $\underline{\underline{\tilde{\beta}}} = -\underline{\underline{\underline{\underline{\tilde{C}}}}}: \underline{\underline{\bar{\varepsilon}}}^{hygro}$ and $\underline{\underline{\tilde{\alpha}}}$ denote the effective hydric stress tensor and the effective hygro-expansion tensor, respectively. The effective tensor of elastic moduli $\underline{\underline{\underline{\underline{\tilde{C}}}}}$ has already be determined by the homogenization numerical procedure described in Section 2. The effective stress tensor is simply computed by applying a uniform hydric unitary load $\Delta h = 1$ together with a zero macroscopic strain $\underline{\underline{\bar{\varepsilon}}} = 0$. For such a loading, $\underline{\underline{\tilde{\beta}}}$ corresponds to the macroscopic stress $\underline{\underline{\bar{\sigma}}}$ which is determined by making the average of the local stress field (5) obtained by solving the local problem (4) through FE simulations. Once $\underline{\underline{\tilde{\beta}}}$ is determined, the effective hygro-expansion tensor $\underline{\underline{\tilde{\alpha}}}$ is derived by the following relation

$$\underline{\underline{\tilde{\alpha}}} = -\underline{\underline{\underline{\underline{\tilde{C}}}}}^{-1}: \underline{\underline{\tilde{\beta}}} \tag{18}$$

In the sequel, it is assumed that the local hygro-expansion tensors $\underline{\underline{\alpha}}^M$ and $\underline{\underline{\alpha}}^F$ are isotropic for the matrix and transversely isotropic for the fibrils, i.e.

$$\underline{\underline{\alpha}}^M = \begin{pmatrix} \alpha^M & 0 & 0 \\ 0 & \alpha^M & 0 \\ 0 & 0 & \alpha^M \end{pmatrix} \text{ and } \underline{\underline{\alpha}}^F = \begin{pmatrix} \alpha_L^F & 0 & 0 \\ 0 & \alpha_{TT}^F & 0 \\ 0 & 0 & \alpha_{TT}^F \end{pmatrix} \tag{19}$$

For such local hygro-expansion tensors, because of the symmetry properties highlighted in Sections 2 and 3, the effective hydric behavior is orthotropic, i.e.

$$\underline{\underline{\tilde{\alpha}}} = \begin{pmatrix} \tilde{\alpha}_1 & 0 & 0 \\ 0 & \tilde{\alpha}_2 & 0 \\ 0 & 0 & \tilde{\alpha}_3 \end{pmatrix} \tag{20}$$

6.2 Comparison of the effective hydric behavior between models 0S, 1S and 2S

Since the local problem (4) is linear, we successively analyze the influence of the fibril oscillations induced by each expansion α^M, $\alpha_L^F, \alpha_{TT}^F$, given an arbitrary value, on the effective hydric properties of the cell wall.

6.2.1 Effect of the swelling of matrix $\alpha^M \neq 0$ ($\alpha_L^F = \alpha_{TT}^F = 0$)

We report in Fig. 20 the evolutions of the normalized effective hydric properties $\tilde{\alpha}_i/\alpha^M (i = 1 \text{ to } 3)$ for the three models as functions of the volume fraction for different values of the shape ratio r_φ. It is observed that the fibril oscillations for both models 1S and 2S have a significant and similar effect on the effective longitudinal hygro-expansion coefficient $\tilde{\alpha}_1$. As expected, this effect increases when the shape ratio decreases. In contrast, only the fibril oscillations of model 2S have a significant effect on the transverse coefficients $\tilde{\alpha}_2$, $\tilde{\alpha}_3$ since models 1S and 0S lead to similar results.

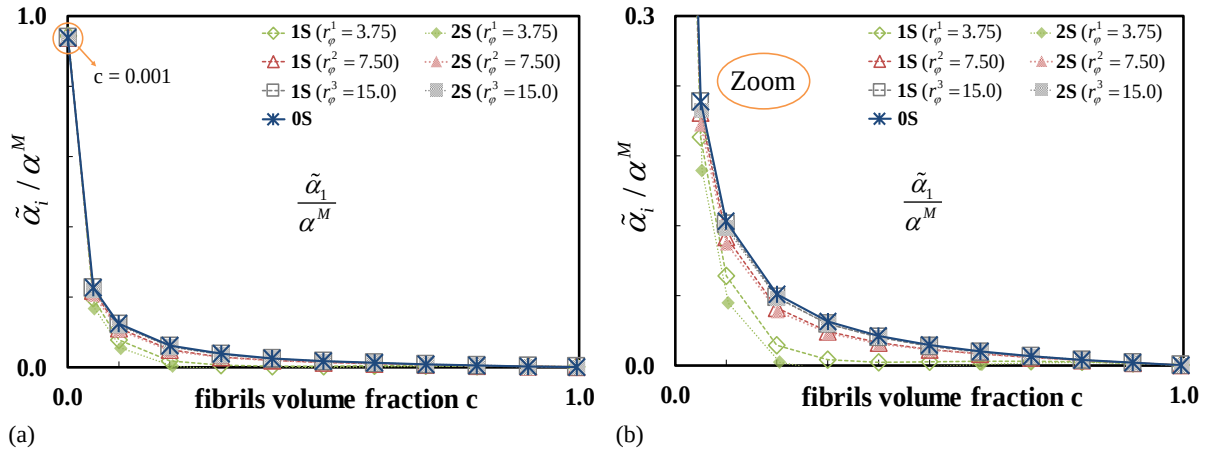

(a) (b)

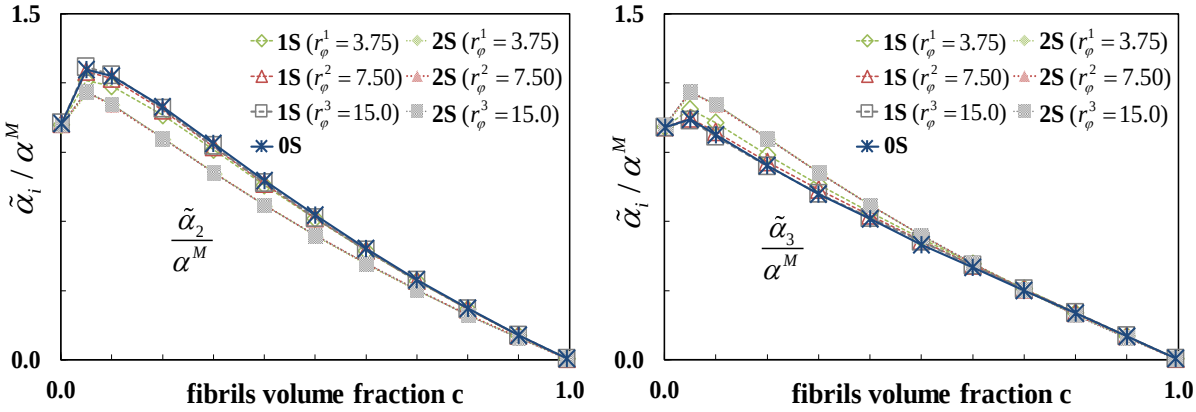

(c) (d)

Fig. 20 Evolutions of the effective hygro-expansion coefficients with respect to the fibrils volume fraction ($\alpha^M \neq 0; \alpha_L^F = \alpha_{TT}^F = 0$).

As exemplified in Fig. 21, it should be noted that the microstructures 0S and 1S lead to an orthotropic effective hydric behavior $\tilde{\alpha}_2 \neq \tilde{\alpha}_3$, with a significant gap between $\tilde{\alpha}_2$ and $\tilde{\alpha}_3$, while the microstructure 2S provides a transversely isotropic behavior $\tilde{\alpha}_2 = \tilde{\alpha}_3$ which is bounded above and below by the transverse hygro-expansion coefficients obtained by model 0S, i.e. $\tilde{\alpha}_3^{0S} \leq \tilde{\alpha}_2^{2S} = \tilde{\alpha}_3^{2S} \leq \tilde{\alpha}_2^{0S}$.

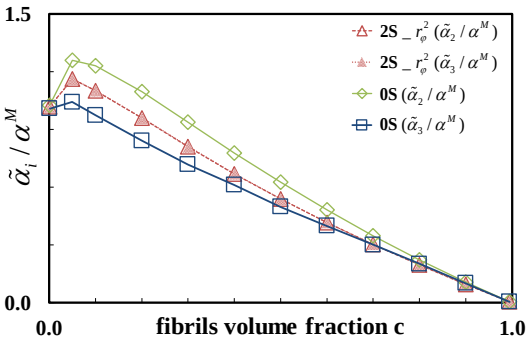

Fig. 21 Evolutions of the effective hygro-expansion coefficients $\tilde{\alpha}_2$ and $\tilde{\alpha}_3$ as functions of the fibrils volume fraction for both model 0S and 2S at r_φ = 7.50 ($\alpha^M \neq 0; \alpha_L^F = \alpha_{TT}^F = 0$)

Lastly, we observe in Fig. 20 (c, d) and Fig. 21 that the effective hygro-expansion coefficients $\tilde{\alpha}_2$ and $\tilde{\alpha}_3$ have values greater than α^M for certain values of the volume fraction. Such an effect is due to the Poisson ratio of the matrix ν^M. Indeed, we numerically observe that this effect disappears as soon as ν^M tends to zero.

6.2.2 Effects of the swelling of fibrils

In this section, we analyze the effects of the swelling of the fibrils on the effective hydric behavior of the cell wall by considering two cases. In the first case, only the longitudinal fibrils expansion is taken into account ($\alpha^M = 0; \alpha_L^F \neq 0, \alpha_{TT}^F = 0$) while in the second case we only consider the transverse hygro-expansion coefficient ($\alpha^M = 0; \alpha_L^F = 0, \alpha_{TT}^F \neq 0$).

a) Case $\alpha_L^F \neq 0$

Similarly to section 6.2.1, we reported in Fig. 22 the variations of the normalized hygro-expansion coefficients with respect to the volume fraction for different values of the shape ratio.

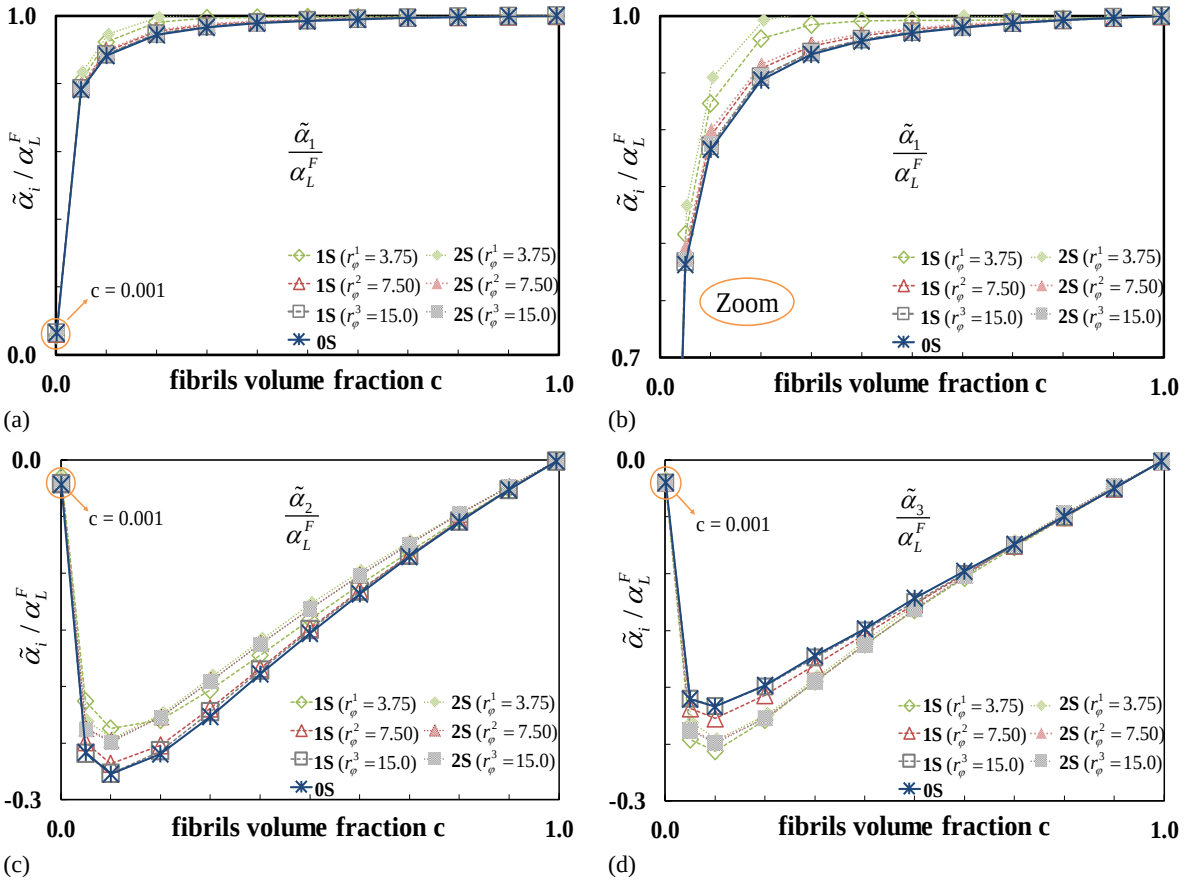

Fig. 22 Evolutions of the effective hygro-expansion coefficients as functions of the fibrils volume fraction. ($\alpha^M = \alpha_{TT}^F = 0; \alpha_L^F \neq 0$).

First, we observe that the fibril oscillations for both model 1S and 2S have a rather weak and similar effect on the effective longitudinal hygro-expansion coefficient $\tilde{\alpha}_1$, and this effect increases when the shape ratio r_φ decreases. For the effective transverse hygro-expansion coefficients $\tilde{\alpha}_2, \tilde{\alpha}_3$, the effect of the fibrils oscillations for both models 1S and 2S is significant. It is worth noting that, as intuitively expected, this effect increases for the model 1S when the shape ratio decreases. However, it does not depend on the shape ratio for the microstructure 2S. As explained in Section 5.3, this latter effect is due to the heterogeneous spatial distribution of the matrix between the oscillating fibrils. Lastly, it should be noted that again the microstructure 0S leads to an orthotropic effective hydric behavior $\tilde{\alpha}_2 \neq \tilde{\alpha}_3$, with a significant gap $\tilde{\alpha}_3$ - $\tilde{\alpha}_2$, while the microstructure 2S provides a transversely isotropic behavior $\tilde{\alpha}_2 = \tilde{\alpha}_3$ which is also bounded by the transverse hygro-expansion coefficients obtained by model 0S, i.e. $\tilde{\alpha}_2^{0S} \leq \tilde{\alpha}_2^{2S} = \tilde{\alpha}_3^{2S} \leq \tilde{\alpha}_3^{0S}$.

b) Case $\alpha_{TT}^F \neq 0$

Again, we reported in Fig. 23 the evolutions of the normalized effective hygro-expansion coefficients with respect to c. It is observed that the fibrils transverse swelling has no influence on the effective longitudinal hygro-expansion coefficient $\tilde{\alpha}_1$ since the values of the latter are almost zero.

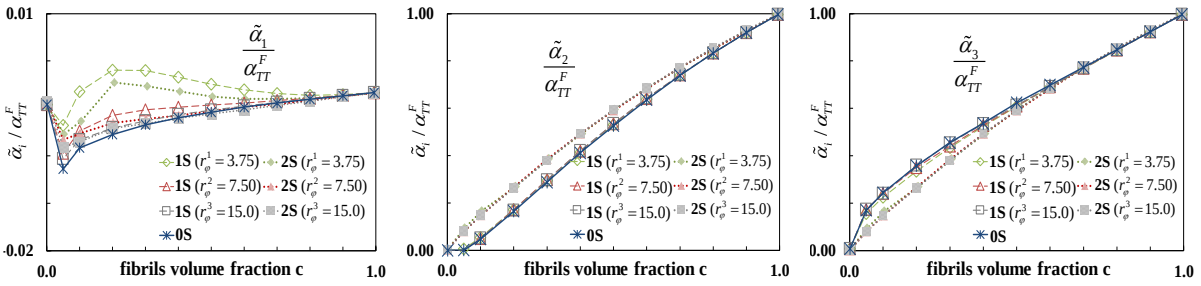

(a) (b) (c)

Fig. 23 Evolutions of the effective hygro-expansion coefficients as functions of the fibrils volume fraction ($\alpha^M = \alpha_L^F = 0; \alpha_{TT}^F \neq 0$).

Furthermore, we observe that the fibrils oscillations associated with microstructure 1S have no influence on the effective transverse hygro-expansion coefficients $\tilde{\alpha}_2, \tilde{\alpha}_3$ since both models 0S and 1S provide the same results. In contrast, the fibrils oscillations associated with microstructure 2S have a significant effect on the effective transverse hygro-expansion coefficients, even if this effect does not depend on the shape ratio and, as seen in Section 5.3, is probably originated from the heterogeneous spatial distribution of the matrix between the oscillating fibrils. Lastly and once again, the model 0S provides an effective orthotropic behavior $\tilde{\alpha}_2 \neq \tilde{\alpha}_3$ with a significant gap between $\tilde{\alpha}_2$ and $\tilde{\alpha}_3$ while the model 2S yields an effective transversely isotropic hydric behavior $\tilde{\alpha}_2 = \tilde{\alpha}_3$ which is bounded by the transverse hygro-expansion coefficients obtained by the model 0S, i.e. $\tilde{\alpha}_2^{0S} \leq \tilde{\alpha}_2^{2S} = \tilde{\alpha}_3^{2S} \leq \tilde{\alpha}_3^{0S}$.

7 Conclusions and perspectives

Two models of microstructure, 1S and 2S, avec been developed using a classical periodic numerical homogenization procedure to evaluate the effect of fibrils oscillations and connections on the effective hygro-mechanical behavior of the cell wall of wood. They were compared with the 0S reference where fibrils are straight and parallel to each other. For the model 1S, the fibrils are allowed to oscillate in the plane (1, 2) while they can oscillate in both planes (1, 2) and (1, 3) for the model 2S. A parametric study was conducted by varying different geometrical and material parameters such as the shape ratio, the volume fraction and the elastic contrast between the matrix and the fibrils. The results obtained are the following.

- Both models 1S and 2S have a significant and nearly same effect on the effective coefficients $\widetilde{C}_{12}$ and $\widetilde{C}_{66} = \widetilde{G}_{12}$ - or equivalently $\widetilde{G}_{12}$ and $\tilde{\nu}_{12}$.

- Only the model 2S is able to take into account the influence of the fibrils oscillations in the plane (1, 3) and also in the transverse plane (2, 3)

- Fibrils oscillations for both microstructures 1S and 2S have nearly no effect on the effective moduli $\widetilde{C}_{11}$, $\widetilde{C}_{22}$, $\widetilde{C}_{33}$ - or equivalently $\widetilde{E}_1$, $\widetilde{E}_2$, $\widetilde{E}_3$.

- For both models 1S and 2S, matrix swelling α^M or axial fibril swelling α_{LL}^F have a significant effect on the axial coefficient $\tilde{\alpha}_1$ but not the transverse swelling of fibrils α_{TT}^F that has a negligible influence.

- For the transverse hygro-expansion $\tilde{\alpha}_2, \tilde{\alpha}_3$ models 1S and 0S provide nearly the same results, thus showing little effect of the fibrils oscillations of microstructure, while model 2S has a significant influence

- Model 1S has an orthotropic hygro-expansion, $\tilde{\alpha}_2 \neq \tilde{\alpha}_3$ with a significant gap between $\tilde{\alpha}_2$ and $\tilde{\alpha}_3$, while model 2S is transversely isotropic for the hydric behavior $\tilde{\alpha}_2 = \tilde{\alpha}_3$, with $\tilde{\alpha}_3^{0S} \leq \tilde{\alpha}_2^{2S} = \tilde{\alpha}_3^{2S} \leq \tilde{\alpha}_2^{0S}$ for the swelling induced by the matrix and $\tilde{\alpha}_2^{0S} \leq \tilde{\alpha}_2^{2S} = \tilde{\alpha}_3^{2S} \leq \tilde{\alpha}_3^{0S}$ for the swellings induced by the fibrils.

The next step of this work consists in making two additional scale transitions in order to evaluate the influence of the fibrils oscillations not only on the cell wall but also in a first time on the elementary woody cells, and then on the growth rings made of early wood and late wood. Such a work is in progress. However, it can be anticipated that the effect of oscillations and cross-linking will be attenuated by the antisymmetric inclination of microfibrils in adjacent cells walls, especially in the case of light wood, such as the earlywood of softwoods, where the cell-wall thickness is smallest. The effect is more likely to be significant for the densest wood where the interaction between the adjacent cell walls is less dominant.

Acknowledgment

Joseph Gril is grateful to Sabine Caré for fruitful discussions that led to reconsider lenticular zones as lignin-xylan incrustations.

References

1. Terashima, N. and Fukushima, K., 1988. Heterogeneity in formation of lignin—XI: An autoradiographic study of the heterogeneous formation and structure of pine lignin. Wood Sci. Technol. 22, pp.259-270.
2. Harrington, J.J., 2002. Hierarchical modelling of softwood hygro-elastic properties. University of Canterbury, Christchurch, New Zealand.
3. Rafsanjani Abbasi, A., 2013. Multiscale poroelastic model - Bridging the gap from cellular to macroscopic scale (Doctor of Sciences). ETH Zurich.
4. Cave, I., 1968. The anisotropic elasticity of the plant cell wall. Wood science and technology 2, pp.268–278.
5. Salmén L., de Ruvo A., 1985. A model for the prediction of fiber elasticity, Wood Fiber Science 17(3), pp.336-350.
6. Persson, K., 2000. Micromechanical modelling of wood and fibre properties (Structural Mechanics). Lund University, Sweden. Department of Mechanics and Materials.
7. Thuvander, F., Kifetew, G. and Berglund, L.A., 2002. Modeling of cell wall drying stresses in wood. Wood Science and Technology, 36(3), pp.241-254.
8. Hofstetter, K. and Gamstedt, E.K., 2009. Hierarchical modelling of microstructural effects on mechanical properties of wood. A review COST Action E35 2004–2008: Wood machining–micromechanics and fracture.
9. Salmén, L., 2004. Micromechanical understanding of the cell-wall structure. Comptes Rendus Biologies 327, pp.873–880.
10. Bardage, S., Donaldson, L., Tokoh, C. and Daniel, G., 2004. Ultrastructure of the cell wall of unbeaten Norwayspruce pulp fibre surfaces. Nordic Pulp & Paper Research Journal 19 (4), pp.448–452.
11. Salmén, L., Stevanic, J.S., Holmqvist, C. and Yu, S., 2021. Moisture induced straining of the cellulosic microfibril. Cellulose, 28(6), pp.3347-3357.
12. Salmén, L. and Burgert, I., 2009. Cell wall features with regard to mechanical performance. A review COST Action E35 2004–2008: Wood machining–micromechanics and fracture.
13. Boyd, J.D., 1982. An anatomical explanation for visco-elastic and mechano-sorptive creep in wood, and effects of loading rate on strength. New Perspectives in Wood Anatomy, pp.171–222. Springer, Dordrecht.
14. Gril, J., 1988. Une modélisation du comportement hygro-rhéologique du bois à partir de sa microstructure (Doctoral dissertation, Paris 6).
15. Reza, M., Ruokolainen, J. and Vourinen, T., 2014. Out-of-plane orientation of cellulose elementary fibrils on spruce tracheid wall based on imaging with high-resolution transmission electron microscopy. Planta 240 (3), pp.565–573.
16. Goring, D.A., 1963. Thermal softening of lignin, hemicelluolose and cellulose. Pulp Pap, pp.517-527.
17. Norimoto, M. and Gril, J., 1989. Wood bending using microwave heating. Journal of microwave power and electromagnetic energy, 24(4), pp.203-212.
18. Inoue, M., Aoki, T. and Egawa, G., 1992. Development of a new teaching material utilizing recovery of compressive set of wood. Wood Research and Technical Notes, 28, pp.59-71.
19. Bornert, M., Bretheau, T. and Gilormini, P., 2001. Homogénéisation en mécanique des matériaux, Tome 1: Matériaux aléatoires élastiques et milieux périodiques (pp. 250-pages). Hermes science.
20. Tang, R.C. and Hsu, N.N., 1973. Analysis of the relationship between microstructure and elastic properties of the cell wall. Wood and Fiber science, 5(2), pp.139-151.
21. Ruel, K., Barnould, F. and Eriksson, E., 1984. Ultrastructural Aspects of Wood Degradation by Sporotrichum pulverulentum - Observations on Spruce Wood Impregnated with Glucose. Holzforschung 38, 61–68.
22. Cristian Neagu, R., Kristofer Gamstedt, E., Bardage, S.L. and Lindström, M., 2006. Ultrastructural features affecting mechanical properties of wood fibres. Wood Material Science and Engineering, 1(3-4), pp.146-170.
23. Nishino, T., Takano, K. and Nakamae, K., 1995. Elastic modulus of the crystalline regions of cellulose polymorphs. Journal of Polymer Science Part B: Polymer Physics, 33(11), pp.1647-1651.
24. Mark, R., 1967. Cell wall mechanics of tracheids, Yale University Press. New Haven, USA.
25. Cave, I.D., 1978. Modelling moisture-related mechanical properties of wood Part I: Properties of the wood constituents. Wood science and technology, 12(1), pp.75-86.
26. Cousins, W.J., 1978. Young's modulus of hemicellulose as related to moisture content. Wood science and technology, 12(3), pp.161-167.
27. Bodig, J., Jayne, B., 1982. Mechanics of wood and wood composites, Van Nostrand Reinhold. ed, Colección general Biblioteca.

+ Bonnet, M.: "Multiscale analysis of the hygromechanical behavior of wood: highlighting the influence of the growth-ring heterogeneity by proton relaxometry and volumetric full-field measurements". Doctoral thesis, Université Paris-Est, in French (2017)

Appendix

Appendix A: components of the tensor of compliance

For an orthotropic elastic behavior, the expression of the components of the compliance tensor $\underline{\underline{\tilde{S}}}$, as defined by Eq. (9), as functions of the ones of the tensor of elastic moduli $\underline{\underline{\tilde{C}}}$ are given in **Error! Reference source not found.**.

Table 4 Components of the effective compliance for an orthotropic elastic behavior

$\tilde{S}_{11} = \frac{1}{D}\left[\tilde{C}_{22}\tilde{C}_{33} - \left(\tilde{C}_{23}\right)^2\right] = \frac{1}{\tilde{E}_1};$	$\tilde{S}_{12} = \tilde{S}_{21} = \frac{1}{D}\left(\tilde{C}_{23}\tilde{C}_{31} - \tilde{C}_{21}\tilde{C}_{33}\right) = -\frac{\tilde{\nu}_{12}}{\tilde{E}_1};$	
$\tilde{S}_{22} = \frac{1}{D}\left[\tilde{C}_{33}\tilde{C}_{11} - \left(\tilde{C}_{31}\right)^2\right] = \frac{1}{\tilde{E}_2};$	$\tilde{S}_{13} = \tilde{S}_{31} = \frac{1}{D}\left(\tilde{C}_{12}\tilde{C}_{23} - \tilde{C}_{13}\tilde{C}_{22}\right) = -\frac{\tilde{\nu}_{13}}{\tilde{E}_1};$	
$\tilde{S}_{33} = \frac{1}{D}\left[\tilde{C}_{11}\tilde{C}_{22} - \left(\tilde{C}_{12}\right)^2\right] = \frac{1}{\tilde{E}_3};$	$\tilde{S}_{32} = \tilde{S}_{23} = \frac{1}{D}\left(\tilde{C}_{31}\tilde{C}_{12} - \tilde{C}_{32}\tilde{C}_{11}\right) = -\frac{\tilde{\nu}_{23}}{\tilde{E}_2};$	
$\tilde{S}_{44} = \frac{1}{\tilde{C}_{44}} = \frac{1}{\tilde{G}_{23}};$	$\tilde{S}_{55} = \frac{1}{\tilde{C}_{55}} = \frac{1}{\tilde{G}_{13}};$	$\tilde{S}_{66} = \frac{1}{\tilde{C}_{66}} = \frac{1}{\tilde{G}_{12}};$
$D = \tilde{C}_{11}\tilde{C}_{22}\tilde{C}_{33} + 2\tilde{C}_{12}\tilde{C}_{23}\tilde{C}_{31} - \tilde{C}_{11}\left(\tilde{C}_{23}\right)^2 - \tilde{C}_{22}\left(\tilde{C}_{31}\right)^2 - \tilde{C}_{33}\left(\tilde{C}_{12}\right)^2;$		